

FINAL REPORT

DOE Contract Number DE-AC21-83MC20013

Laboratory Analysis of Gas Hydrate
Cores for Evaluation of Reservoir Conditions

June 1984

Submitted By

G. D. Holder
Principal Investigator

ABSTRACT

Methodology and procedures for the study of hydrate cores are detailed. Topics discussed are the 1) equipment and procedures for the formation and evaluation of hydrate cores in the laboratory, 2) the thermodynamic properties of gas hydrates, 3) the enthalpy of hydrate dissociation, 4) conditions in the earth where hydrates can form, 5) kinetics of hydrate formation and dissociation, and 6) heat transfer to gas hydrates. Empirical correlations for these properties and kinetic behavior are given.

TABLE OF CONTENTS

Abstract	i
List of Figures	iii
List of Tables	vi
Introduction	1
Statement of Work	2
Results	
1. Design of an Apparatus for the Formation of Hydrate Cores	3
2. Conditions and Procedures for Formation of Hydrate Cores	6
3. Procedure for Formatio'n of Hydrate Cores in Terms of Porosity, Hydrate Fraction, and Ice Fraction in Terms of Formation Conditions and Formation Time	9
4. Thermodynamic Properties of Gas Hydrates	12
5. Enthalpies of Hydrate Formation.....	25
6. Heat Transfer Between Hydrates and a Warm Bulk Fluid	39
7. Analysis of Reservoir Conditions where Hydrates are Likely to Form	64
8. Advice and Consultation.....	80
References	82

LIST OF FIGURES

Figure 1	Hydrate Formation Cell.....	4
Figure 2	Hydrate Formation Rates.....	8
Figure 3	Hydrate Conversion as a Function of Pressure.....	10
Figure 4	The Effect of Carbon Dioxide on the Hydrate Dissociation Pressure of a Methane-Rich Gas.....	13
Figure 5	The Effect of Hydrogen Sulfide on the Dissociation Pressure of a Methane-Rich Gas.....	14
Figure 6	The Effect of Nitrogen on the Hydrate Dissociation Pressure of a Methane-Rich Gas.....	15
Figure 7	The Effect of Ethane on the Hydrate Dissociation Pressure of a Methane-Rich Gas.....	16
Figure 8	The Effect of Carbon Dioxide on the Hydrate Dissociation Pressure of a Methane + Ethane Mixture.....	17
Figure 9	The Effect of Carbon Dioxide on the Hydrate Dissociation Pressure of a Methane + Ethane Mixture.....	18
Figure 10	The Effect of Hydrogen Sulfide on the Hydrate Dissociation Pressure of a Methane + Carbon Dioxide Mixture.....	19
Figure 11	The Effect of Carbon Dioxide on the Hydrate Dissociation Pressure of a Methane + Ethane + Propane Gas Mixture.....	20
Figure 12	Temperature Dependence of Dissociation Pressure Coefficient, A.....	23
Figure 13	Temperature Dependence of Dissociation Pressure Coefficient, B.....	24
Figure 14	The Effect of Ethane on the Hydrate Dissociation Enthalpy in a Methane-Rich Gas.....	28
Figure 15	The Effect of Carbon Dioxide on the Hydrate Dissociation Enthalpy in a Methane-Rich Gas.....	29
Figure 16	The Effect of Hydrogen Sulfide on the Hydrate Dissociation Pressure of a Methane-Rich Gas.....	30
Figure 17	The Effect of Nitrogen on the Hydrate Dissociation Enthalpy in a Methane-Rich Gas.....	31
Figure 18	The Effect of Carbon Dioxide on the Hydrate Dissociation Enthalpy of a Methane + Ethane Mixture.....	32

Figure 19	The Effect of Carbon Dioxide on the Hydrate Dissociation Enthalpy of a Methane + Ethane Mixture.....	33
Figure 20.	The Effect of Hydrogen Sulfide on the Hydrate Dissociation Enthalpy of a Methane + Carbon Dioxide Mixture.....	34
Figure 21	The Effect of Carbon Dioxide on the Hydrate Dissociation - Enthalpy in a Methane + Ethane + Propane Mixture.....	35
Figure 22	The Temperature Dependence of the Enthalpy Coefficient, A.....	37
Figure 23	The Temperature Dependence of the Enthalpy Coefficient, B.....	38
Figure 24	Experimental Apparatus.....	41
Figure 25	Comparison of Experimental (Points) and Predicted Conversions (Lines).....	48
Figure 26	Schematic Diagram Representing Temperature Profile For Unsteady State Dissociation.....	50
Figure 27a	Heat Flux Versus Temperature Driving Force for Methane Hydrate Dissociation.....	51
Figure 27b	Rate of Dissociation Versus Temperature Driving Force for Methane Hydrate Dissociation.....	52
Figure 28	Unsteady-State Heat Transfer to Hydrates and Hydrate Dissociation in Unconsolidated Sediment.....	62
Figure 29	Temperature-Depth Profiles for Hydrate Stability Zones, I.....	65
Figure 30	Temperature-Depth Profiles for Hydrate Stability Zones, II.....	66
Figure 31	Temperature-Depth Profiles for Hydrate Stability Zones, III.....	67
Figure 32	The Effect of the Geothermal Gradient Below the Permafrost on the Hydrate Stability Zone Beneath the Permafrost.....	68
Figure 33	The Effect of Permafrost Thickness on the Hydrate Stability Zone Thickness in the Permafrost.....	69
Figure 34	The Effect of Permafrost Thickness on the Thickness of the Hydrate Stability Zones for Seven Gas Compositions.....	70
Figure 35	Depth-Temperature Profiles and Hydrate Stability Curves Beneath the Ocean, I.....	71

Figure 36	Depth-Temperature Profile and Hydrate Stability Curve, Beneath the Ocean, It	72
Figure 37	Depth-Temperature Profile and Hydrate Stability Curves Beneath the Ocean, It	73
Figure 38	The Effect of the Ocean's Depth on the Hydrate Stability Zone Beneath the Ocean	74
Figure 39	The Effect of Ocean Depth on the Thickness of the Zone of Hydrate Stability - Different Gas Compositions.....	75

LIST OF TABLES

Table I	VIR and VLR Dissociation Pressures for Pure Gases.....	12
Table II	Coefficients for Dissociation Pressure Correlations for Gases in Methane	22
Table III	Volume Changes Upon Converting Water to Hydrate.....	25
Table IV	Dissociation Enthalpies of Pure Species	26
Table V	Coefficients for Calculating the Effect of Other Gases on Dissociation Enthalpies	36
Table VI	Summary of Hydrate Formation Runs	43
Table VII	Pressure-Time-Conversion Data.....	44
Table VIII	Variables for Case Study	55
Table IX	Dissociation of Methane Hydrates	63
Table X	Default Values for Hydrate Stability Zone Calculations	76

INTRODUCTION

Gas hydrates are clathrate ices in which each water molecule forms hydrogen bonds with its four nearest neighbors to build a solid lattice which encages a gas molecule in its interstitial cavities. These solid, ice-like mixtures of natural gas and water have been found in rocks beneath the permafrost, in Arctic basins, and in muds under deep water along the continental margins of America. Although they have been known to exist for over a century and half, it was the discovery of natural gas in the "frozen state" in Siberia in the early sixties [1] that stimulated widespread interest in naturally occurring gas hydrates.

Estimates of the quantity of natural gas in the form of hydrates as well as in the gas trapped in zones below the impermeable hydrate zones have been made. Estimates of the amount of hydrated natural gas in the world cover wide range ($1.4 \times 10^{13} \text{ m}^3$ to $7.6 \times 10^{18} \text{ m}^3$) but in all cases are enormous [2-4]. Because of this potential resource, the problems associated with the production of natural gas from these hydrate zones have become of greater interest to the hydrocarbon industries.

Many aspects of gas hydrates have been studied extensively in the past including; (a) hydrate structures [5-7], (b) conditions under which hydrates form or dissociate [8-10], (c) the composition of gas hydrates [11], (d) thermodynamic properties of gas hydrates [12], (e) principles of hydrate inhibition [13], and (f) the natural occurrence of gas hydrates [14]. In addition, preliminary work on modeling production of gas in hydrate form has been done by Makogon et al. [15], Holder et al. [16] and McGuire [17]. However, one area which is important but which has not been studied in the past is the thermodynamic and transport properties of hydrate cores.

STATEMENT OF WORK

The object of this work was to provide technical assistance to METC's effort to develop a leading program in the evaluation of hydrate samples in porous media at reservoir conditions. Below is an outline of each of the goals listed in the scope of work:

1. Design of an apparatus for the formation of hydrate cores.
2. Develop the conditions and procedure for formation of hydrate cores. We have formed hydrate cores in my laboratories at the University of Pittsburgh. We will provide expertise to METC on the technique for forming such cores in the apparatus.
3. Analyze the composition of synthetic hydrate cores in terms of porosity, hydrate fraction, and ice fraction of formation conditions and formation times.
4. Determine thermodynamic properties of hydrates in terms of formation temperatures and pressures. Develop depth versus temperature charts which will indicate where hydrates can form.
5. Determine enthalpies of hydrate dissociation as a function of temperature, pressure, and composition.
6. Determine heat transfer coefficients for heat transfer between dissociating hydrates and a bulk fluid.
7. Conduct an analysis of reservoir conditions (depth, thickness, pressure, temperature, etc.) in the earth where hydrates are likely to form.
8. Provide advice and consultation on current gas hydrates experiments at METC.

RESULTS

The results will be reported by task number as identified above.

1. Design of an apparatus for the Formation of Hydrate Cores

Figure 1 shows an outline of the design of the high pressure vessel to be used. In this design, 4" x 150 lb stainless steel flanges are used. Two slip-on flanges are to be welded to the 4" pipe and two blank flanges are to be bolted on. The pipe should be at least schedule 80 or heavier. Neoprene o-rings are recommended for sealing. Welds are indicated on the drawing. Below are the dimensions of the equipment. All materials are stainless steel (304 or 316).

1. 150# flanges: (4 needed) 1-5/16" thickness, wt. 1S lbs-blank, 10 Lbs slip-on

2. Bolts (16 needed): 1/2" bolts at least 4" in length

3. 4" Pipe (15 inches needed)

schedule 80 (20 lbs) I.D. = 3.826; wall = .337"

schedule 120 (25.5 lbs) I.D. = 3.624" wall = .438"

schedule 160 (30 lbs) I.D. = 3.428" wall = .531"

Based upon these weights the vessel pipe will weigh approximately 70lbs if schedule 80 pipe is used and 80 lbs if schedule 160 pipe is used.

The design pressure for the pipe thickness required is 0.25" for 2000 psi using

$$t = \frac{P.R}{S.E} - 0.6P$$

P = 2000 psi internal pressure

R = Pipe Radius (3.826"/2)

PRESSURE VESSEL

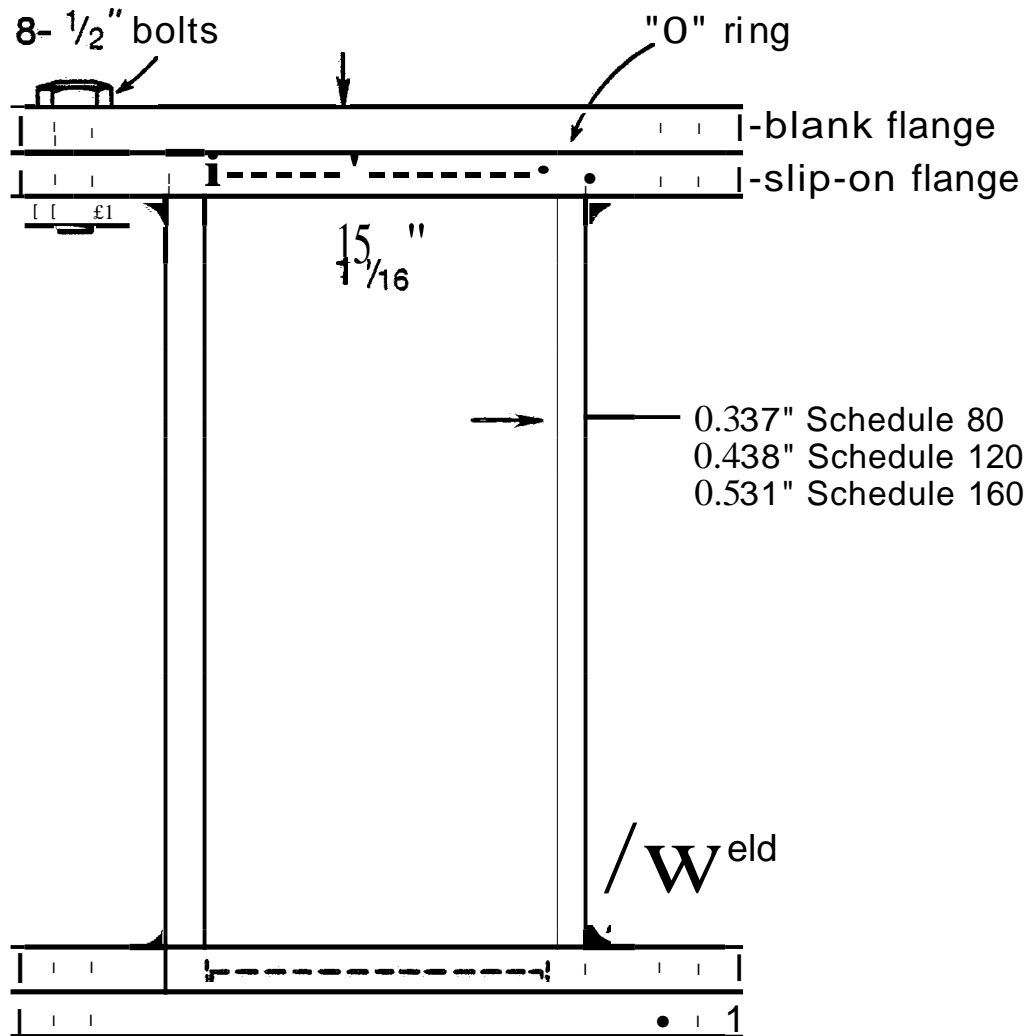


Figure 1. Hydrate Formation Cell

S = Maximum working stress (18,750 psi)

E = Efficiency (0.9)

The flanges have standard ratings of 275 psi working pressure. Pressures higher than this are not recommended since leaks may occur. However, we have used the same design at the University of Pittsburgh at pressures to 1500 psi (occasionally) and with frequent pressures to 1100 psi. The actual design thickness for a welded flat end is 0.78" for 2000 psi as given by

$$t = d \sqrt{\frac{C_s P}{S}}$$

d = Diameter to O-ring (6")

C = Geometric coefficient (0.162)

P = Pressure (2000 psi)

S = Stress allowed (18,750 psi)

The 150 lb flanges are 1.3125" thick which is thicker than the design thickness. If pressures higher than 275 psi are to be used the vessel must be hydrostatically tested to 1.5 times the maximum working pressure at sixty day intervals.

Several ports will be required for the inlet/outlet, RTD's and plungers and/or transducers. These ports can be tapped into the top and bottom flanges as needed. Pressure testing should be done with port already tapped.

Section 6 has a discussion of the entire experimental section in which this pressure vessel is used.

2. Conditions and Procedure for Formation of Hydrate Cores

In order to form hydrates (^{omit} ~~must exist~~) a large interfacial area must exist between the methane gas and the water or ice phase. This is accomplished by forming a core of frost and saturating ^{it} with methane gas) which fills the core of the frost (water-ice).

The frost can be formed by placing a beaker of water in the freezer. The beaker of water should have a heater placed in it to keep the water from freezing. The water will evaporate and condense in fine crystals along the freezer walls. These crystals can be scraped off for forming hydrates. The dry crystals should be placed in a pre-cooled insulated beaker which can be weighed on a top-loading balance. This will allow the weight of the crystals to be determined without their melting.

The recommended procedure for forming methane hydrates is as follows:

Initially, a known quantity of frost (finely divided ice crystals) is charged to the pressure vessel which is kept in a refrigerated bath at low temperatures (-25°C) to prevent melting. The frost should be added in four portions with each portion (of 75g weight) being compacted by a piston prior to adding the next portion. This ensures a uniform void fraction of 0.4 to 0.5. The vessel should then be closed, evacuated and pressurized to 1000-1100 J psia with a known quantity of methane. For purposes of monitoring pressure, an accurate gauge (0-2000 psi) or transducer will be needed. The temperature of the frost zone should be monitored during the process in order to keep it lower than 273.15K, thereby preventing any premature melting of the frost.

After the frost zone is saturated completely with methane, the temperature of the bath should be raised to 274 K and maintained at this temperature for a period generally longer than 24 hours. During this time, nucleation and formation of hydrates takes place. Typical rates are shown in

Figure 2. After the formation of the hydrates, excess methane can be vented. Some additional kinetic discussion is given in Section 6.

The equipment needed for this procedure is

- 1) an accurate pressure gauge (0.25%)
- 2) thermometer (RTD)
- 3) Beaker (1000 ml) for transferring ice crystals
- 4) Piston
- 5) Pressure vessel
- 6) Methane cylinder (2500 psi)
- 7) Freezer
- 8) Submersible 50 watt heater
- 9) Large beaker for freezer water (2000 ml)

FORMATION RATES FOR METHANE HYDRATE

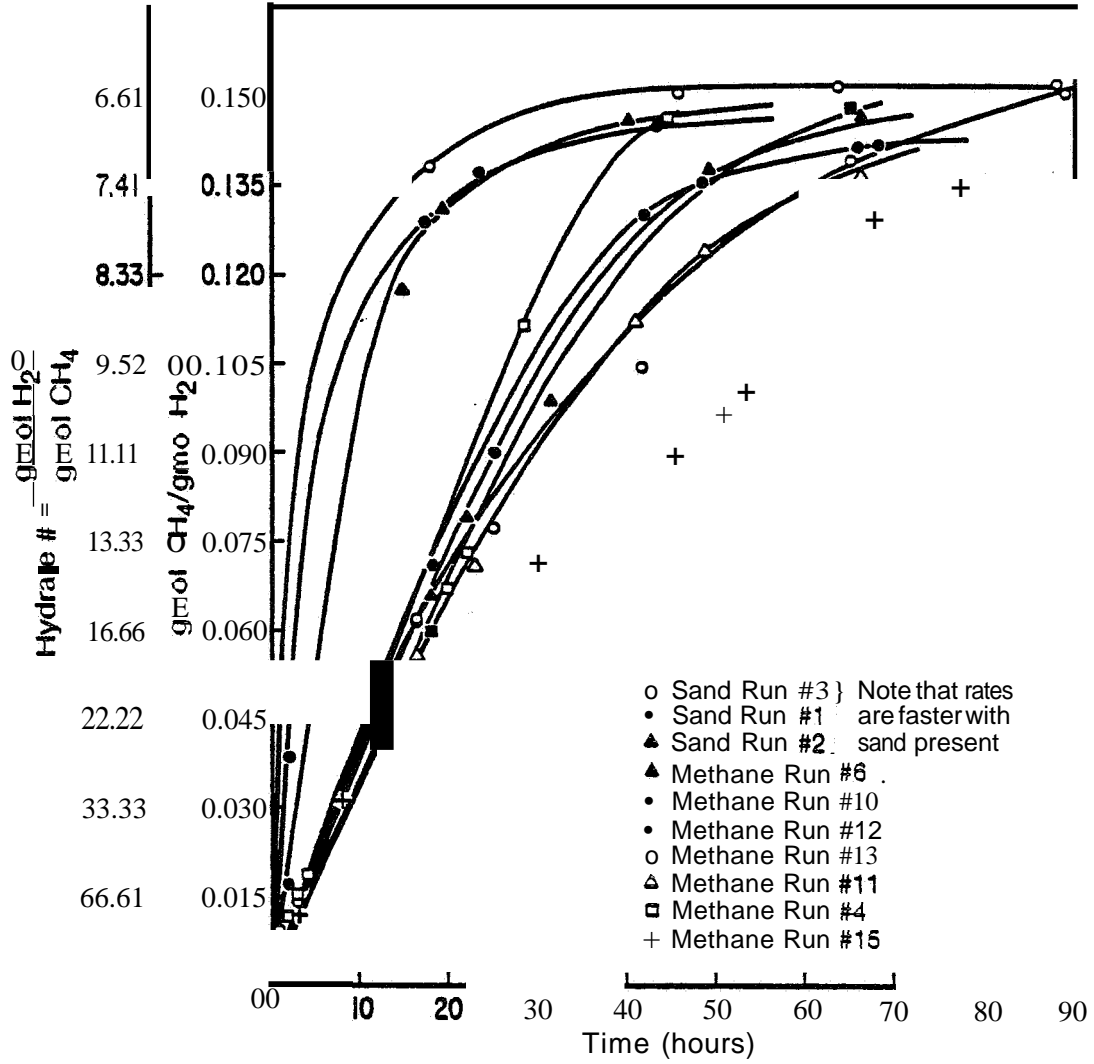


Figure 2. Hydrate Formation Rates

3. Analysis of the Composition of Synthetic Hydrate Cores in Terms of Porosity, Hydrate Fraction, and Ice Fraction in Terms of Formation Conditions and Formation Times

To determine the percent conversion of ice to hydrate, the volume of the pressure vessel and connecting pipe **must** be known. The amount of ice placed in the vessel will take up a known volume (1.09 cc/gm) and the rest will be methane gas. The amount of gas initially in the vessel is determined by

$$\text{number of moles of methane gas} = n_0 = \frac{P(V-VI)}{ZRT} \quad (3-1)$$

where P is the initial pressure (about 1000 psi) it should be measured 30 minutes after charging the gas to allow equilibrium of temperature. V is the volume of the vessel; VI is the volume of ice; Z is the compressibility factor obtained from an equation of state (see Figure 3), and T is the temperature which should be -5°C or lower.

The amount of gas converted to hydrate can be calculated at any subsequent pressure and temperature by applying the above equation. At the new pressure and temperature it will give the amount of gas remaining. The difference (n₀-n) is the number of moles of gas in the hydrate phase. The percent conversion is calculated as

$$\% \text{ conversion to hydrate} = (100) \frac{\text{moles of gas in hydrate phase}^*}{\text{moles of water in vessel}} \cdot 6.15$$

At 100% conversion and at 0°C there should be 6.15 moles of water in the hydrate phase for every mole of gas in the hydrate phase. Figure 2 shows how the conversion depends upon time. Generally 72 hours are sufficient for 90% conversion.

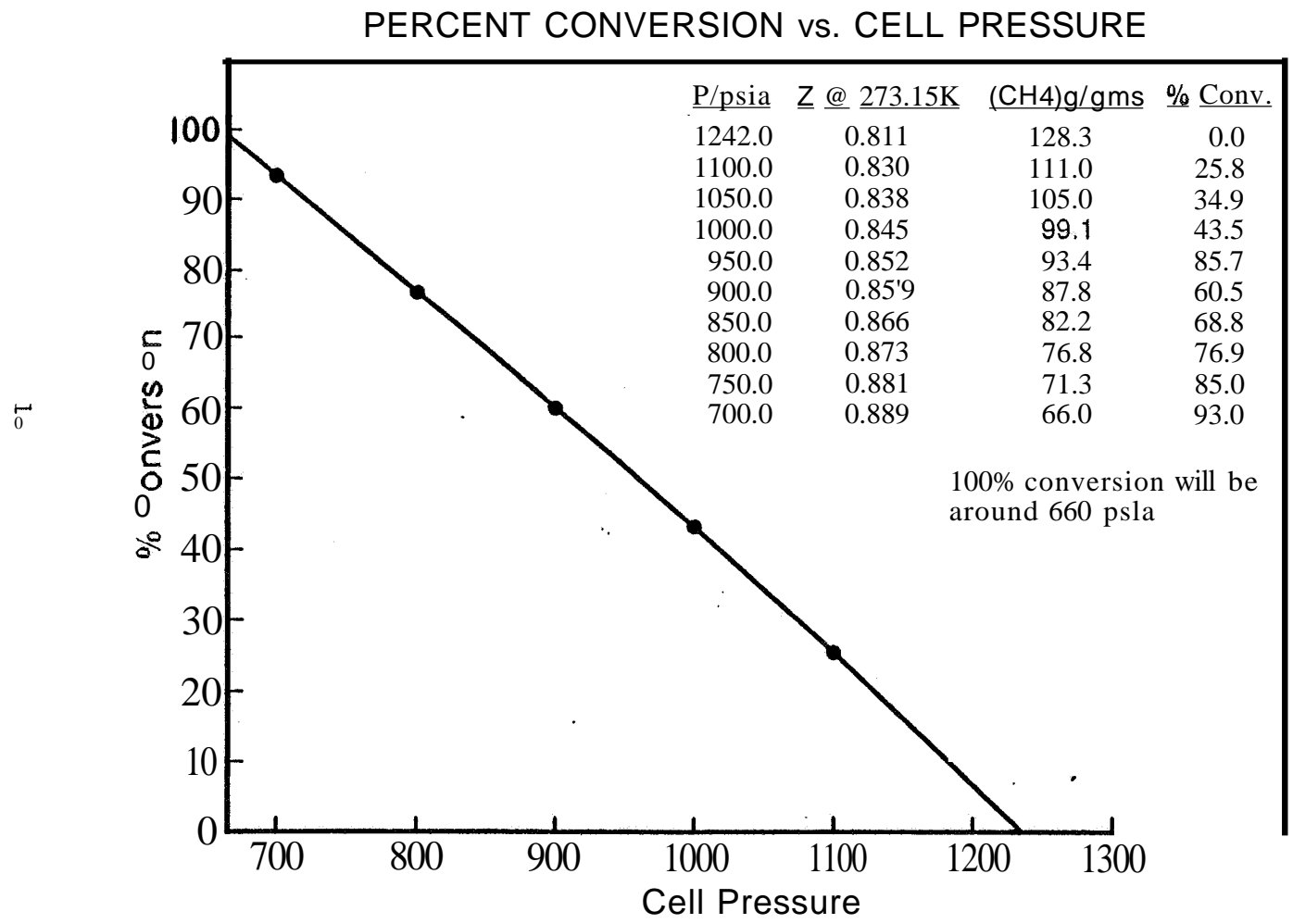


Figure 3. Hydrate Conversion as a Function of Pressure

The attached table shows the information on the hydrate core provided to METC in July, 1983. The stoichiometric methane requirement is the moles of water in the vessel divided by 6.15.

To determine the porosity of the ice core, the mass, m_I of ice charged to the vessel is determined by weighing the ice. The ice is then compacted into the vessel and the empty height, h_E , of the vessel is measured. The bulk volume of ice is thus $V_B = V (h_T - h_E) / h_T$ where h_T is the total vessel height and V is the vessel volume. The ice porosity is then

$$\phi_I = 1 - \frac{m_I}{\rho_I V_B} \quad (3-2)$$

where ρ_I is the density of ice (0.92 g/cc). As hydrates form, the porosity will decrease according to the following

$$\phi = \phi_I + \frac{m_I f}{\rho_I V_I} \left(1 - \frac{\rho_I}{\rho_H} \right) \quad (3-3)$$

where f is the fraction of the ice converted to hydrate and ρ_H is the density of water in the hydrate (0.88 g/cc).

4. Thermodynamic Properties of Gas Hydrates*

Table I below, gives regressions for calculating dissociation pressures of several hydrates along the three phase, VLH and VIH, loci. At a given temperature, the dissociation pressure is the minimum pressure required to form hydrates. At higher pressures, hydrates will form until all of the gas or all of the water is converted to hydrate, whichever comes first.

TABLE I. VIH and VLH Dissociation Pressures for Pure Gases
 $P/\text{kPa} = \exp [a - b/T]$ T in kelvins

GAS	STRUCTURE	a	b	Temp. range
CH ₄	I	14.7170	-1886.79	-25 to 00C
CH ₄	I	38.9803	-8533.80	0° to 25°C
C ₂ H ₆	I	17.5110	-3104.535	-25 to 00C
C ₂ H ₆	I	44.2728	-10424.248	0 to 25°C
C ₃ H ₈	II	17.1560	-32.69.6455	-25 to 00C
C ₃ H ₈	II	67.1301	-16921.84	0 to 00C
CO ₂	I	18.5939	-3161.41	-25 to 00C
CO ₂	I	44.5776	-10245.01	0 to 110C
N ₂	I	15.1289	-1504.276	-25 to 00C
N ₂	I	37.8079	-7688.6255	0 to 25°C
H ₂ S	I	16.5597	-3270.409	-25 to 00C
H ₂ S	I	34.8278	-8266.1023	0 to 25°C

Figures 4-11 show how the dissociation pressure depends upon the presence of other gas species (N₂, H₂S, CO₂, C₂H₆, C₃H₈) in a natural gas consisting

*Depth versus temperature charts are given in Section 6.

CH₄/CO₂ Gas Hydrates

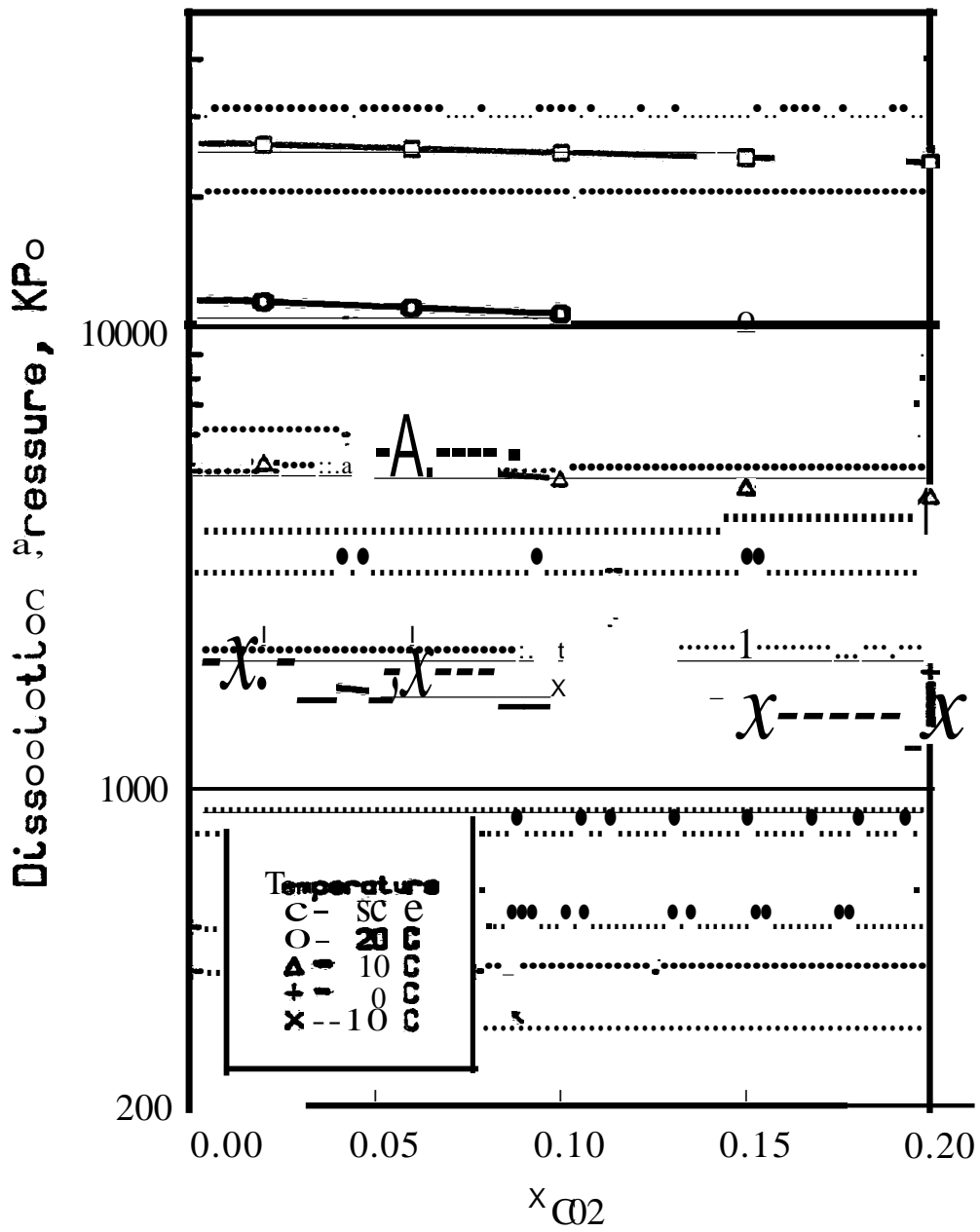


Figure 4: The Effect of Carbon Dioxide on the Hydrate Dissociation Pressure of a Methane-Rich Gas

CH₄/H₂S Gas Hydrates

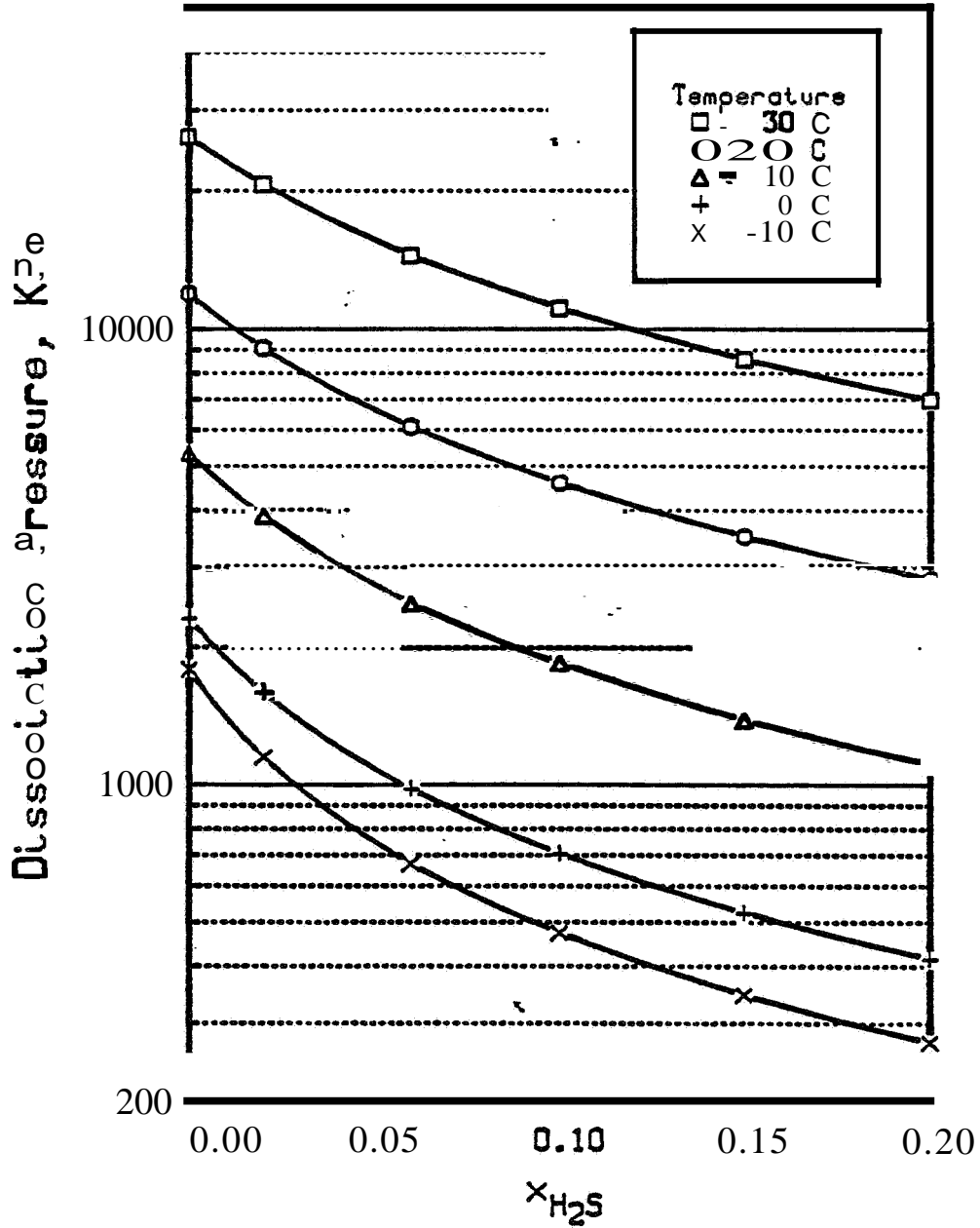


Figure 5: The Effect of Hydrogen Sulfide on the Dissociation Pressure of a Methane-Rich Gas

CH₄/N₂ Gas Hydrates

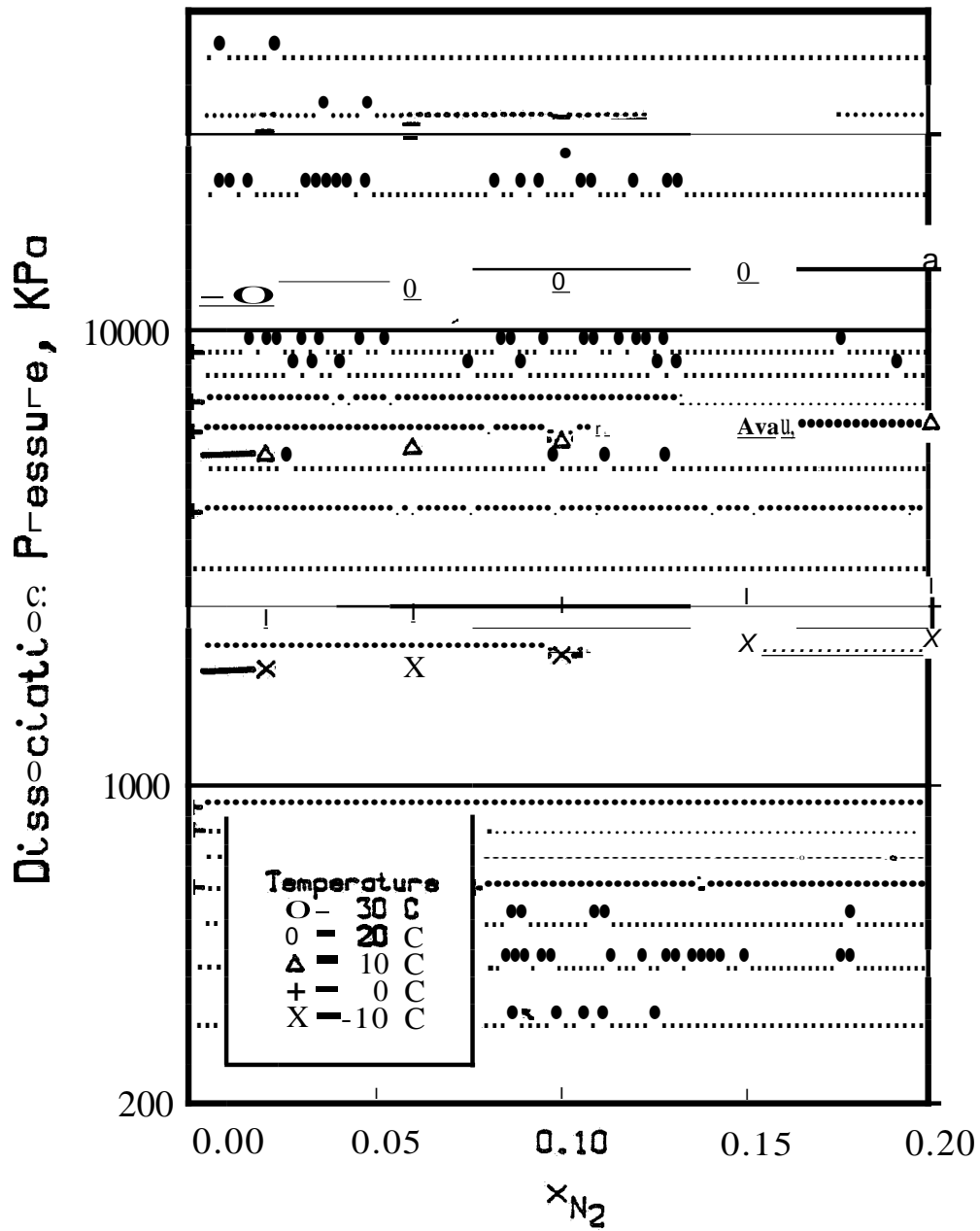


Figure 6: The Effect of Nitrogen on the Hydrate Dissociation Pressure of a Methane-Rich Gas

CH₄/C₂H₆ Gas Hydrates

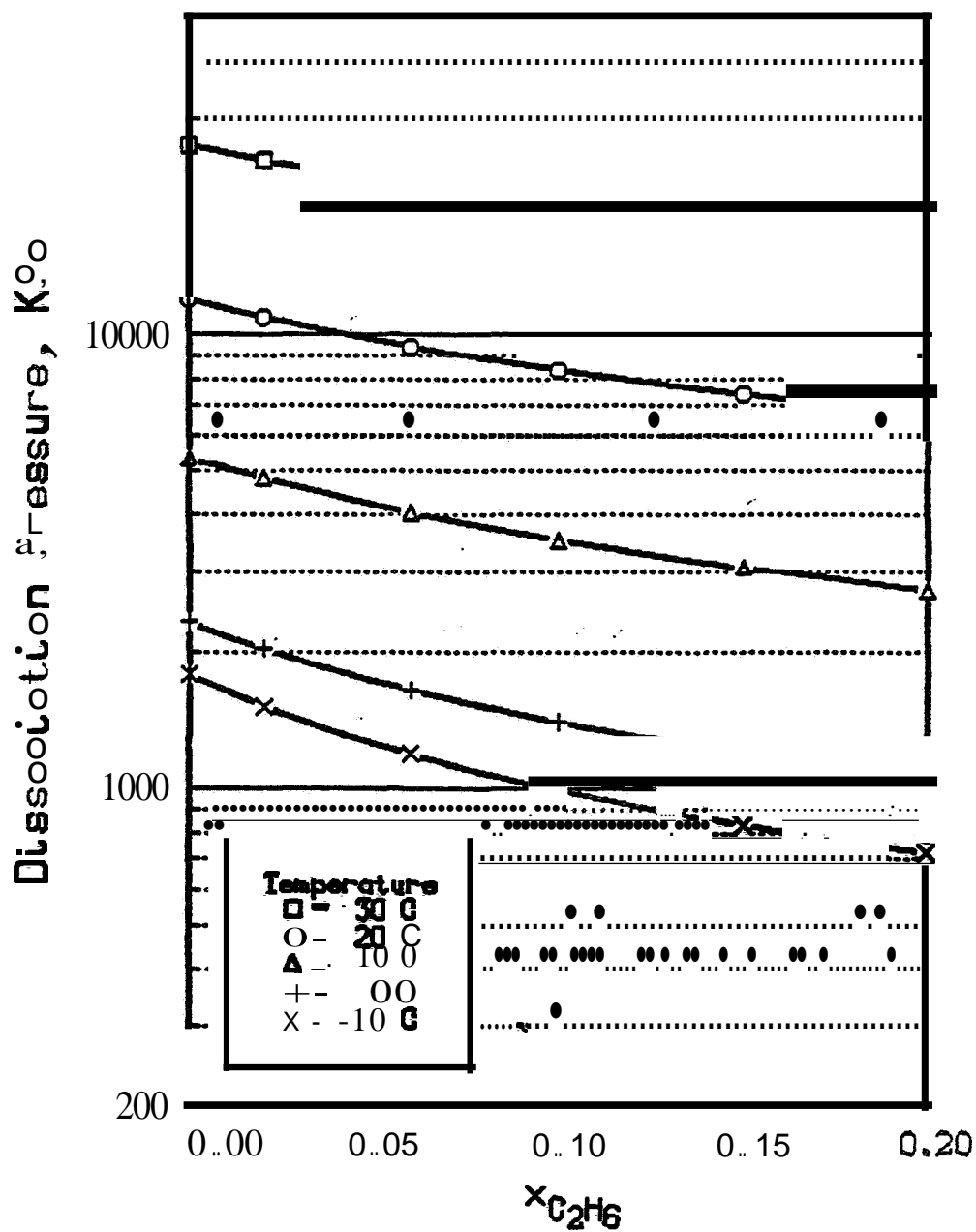


Figure 7: The Effect of Ethane on the Hydrate Dissociation Pressure of a Methane-Rich Gas

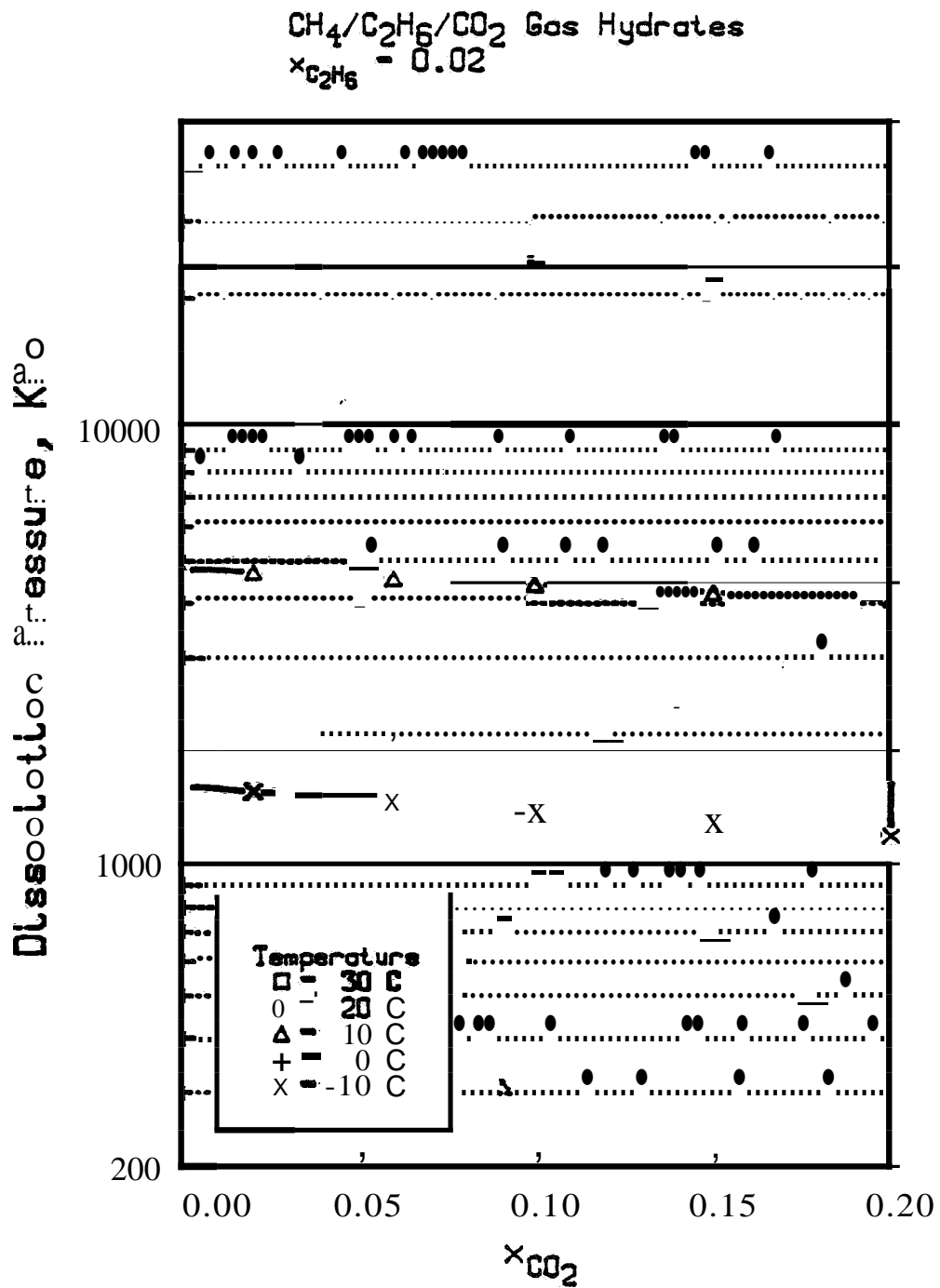


Figure 8: The Effect of Carbon Dioxide on the Hydrate Dissociation Pressure of a Methane + Ethane Mixture

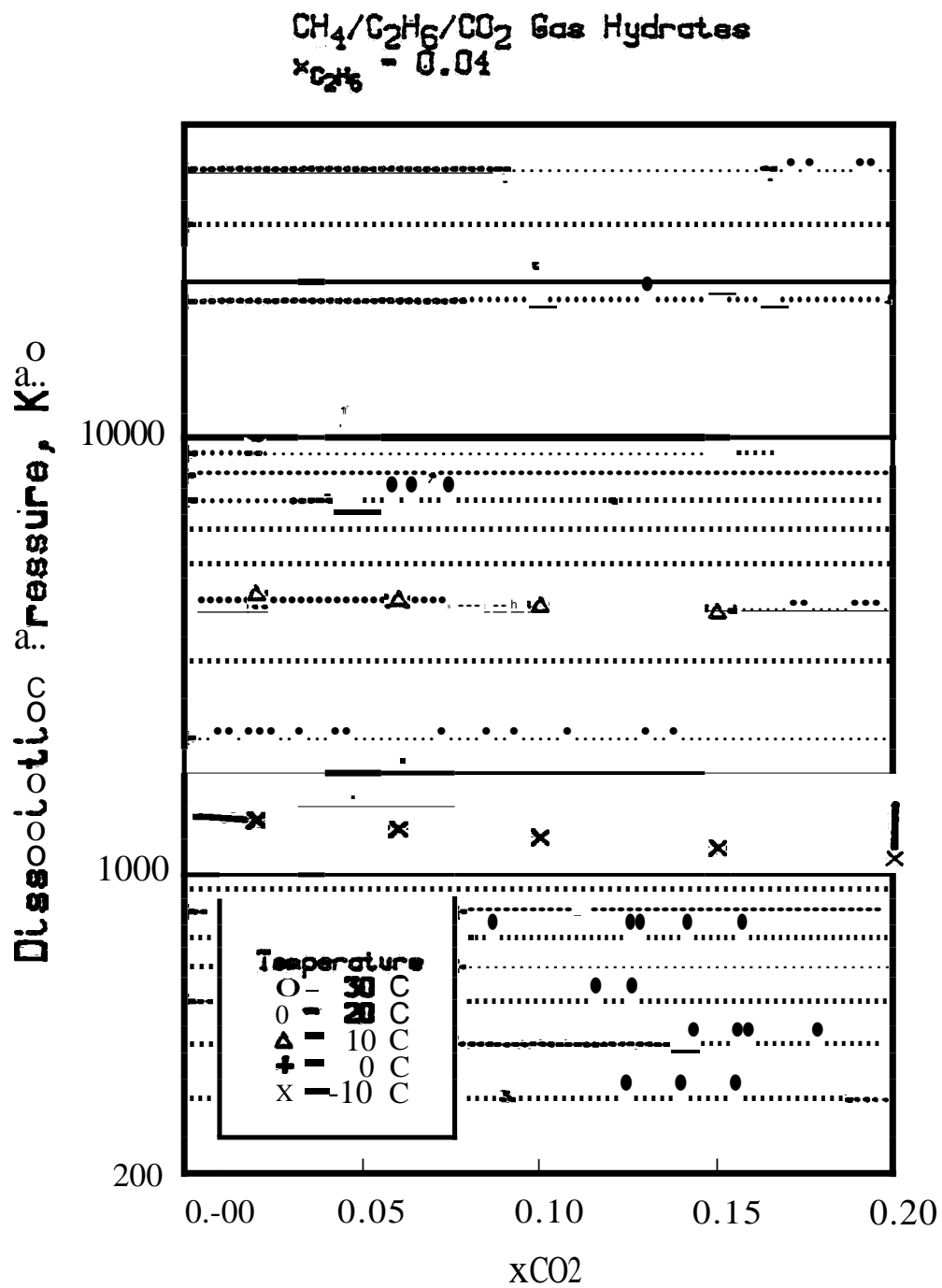


Figure 9: The Effect of Carbon Dioxide on the Hydrate Dissociation Pressure of a Methane + Ethane Mixture

CH₄/CO₂/H₂S Gas Hydrates
 $x_{CO_2} = 0.04$

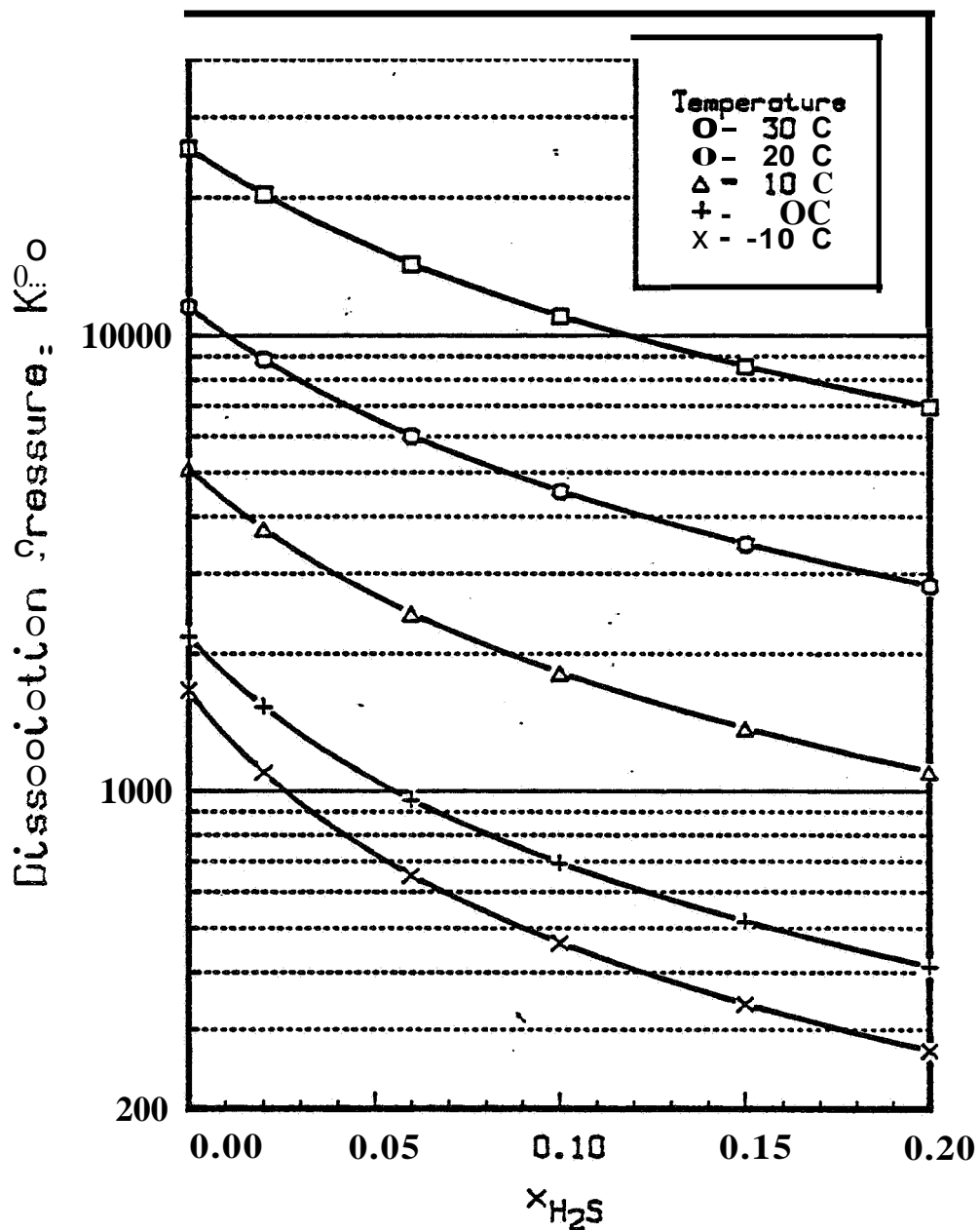


Figure 10: The Effect of Hydrogen Sulfide on the Hydrate Dissociation Pressure of a Methane + Carbon Dioxide Mixture

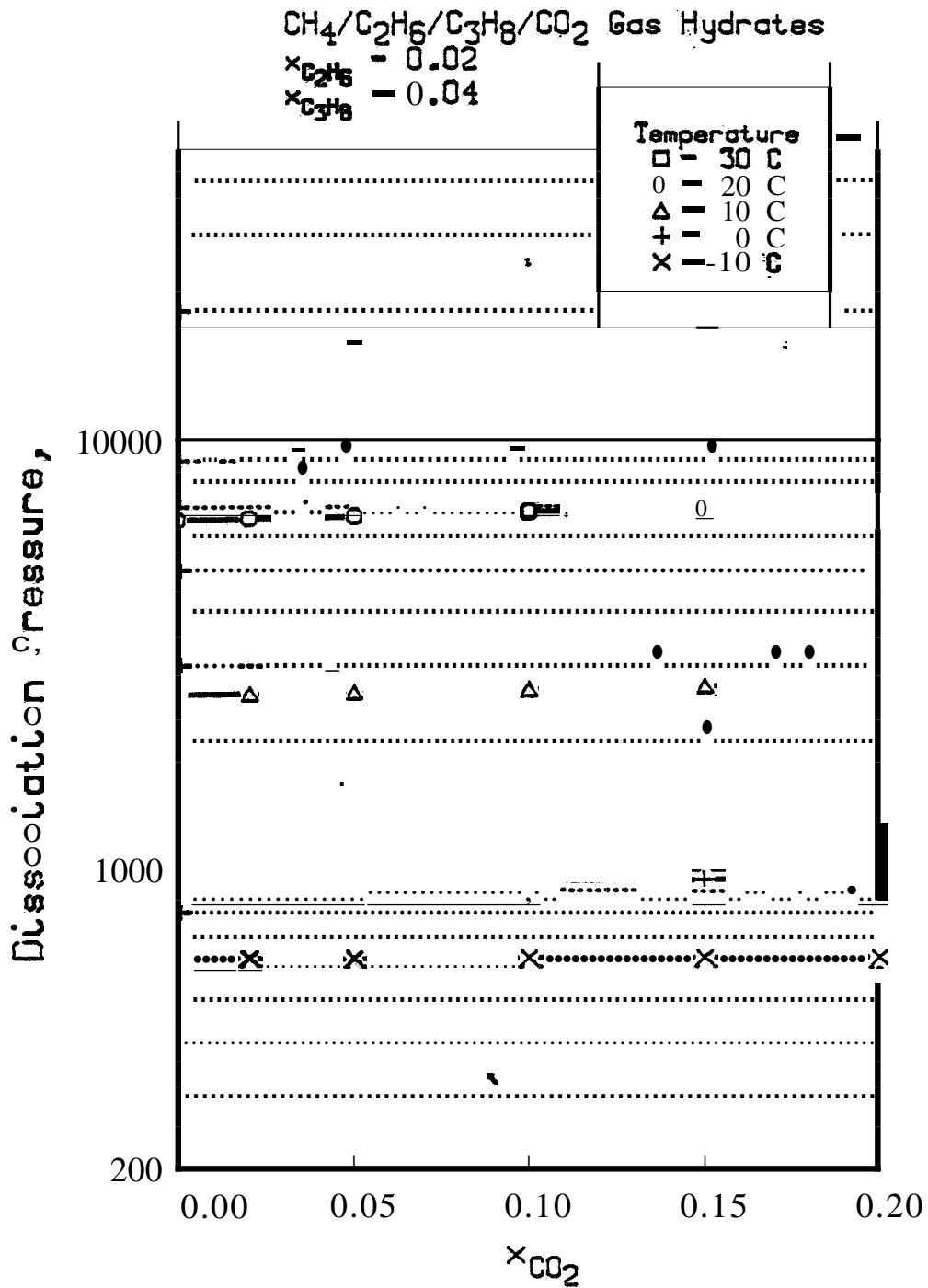


Figure 11: The Effect of Carbon Dioxide on the Hydrate Dissociation Pressure of a Methane + Ethane + Propane Gas Mixture

primarily of methane. The composition and gases given are the most likely to be present in a natural gas. Table II gives coefficients for the following regression

$$\ln (PIP_o) = Ax_2 + Bx_2^2 \quad (4-1)$$

where x_2 is the mole fraction of the second gas in methane. The mole fraction methane is $1-x_2$, the "dissociation pressure of methane hydrate is P_o ' and the dissociation pressure of the hydrate formed from a gas containing $(1-x_2)$ mole fraction methane and x_2 mole fraction of the second species is P . For a mixture the correlation becomes

$$\ln (P/P_o) = \sum (A_i x_i + B_i x_i^2) \quad (4-2)$$

where x_i are the non-methane mole fractions of the hydrate formers present, and the A_i and B_i are their binary coefficients.

Figures 12 and 13 show the temperature dependence of the binary coefficients and can be used for interpolation.

For binary gases these correlations will be quite accurate, but for multicomponent mixtures the correlations are accurate to $\pm 10\%$. Calculations based upon correlations will not be as accurate as are calculations using the algorithms of John and Holder (25), but these correlations provide good estimate of the effect of gas composition.

Table II: Coefficients for Dissociation Pressure Correlations for Gases in Methane

$$\ln P/P_o = Ax + Bx^2$$

TOe	C ₃ H ₈		H ₂ S		C ₂ H ₆		CO ₂		N ₂	
	A	B	A	B	A	B	A	B	A	B
30	-28.56	209.8	-10.62	19.98	-3.698	5.620	-.5797	.3420	.8523	.4390
20	-34.20	256.4	-11.94	23.74	-4.405	8.052	-.8192	.4940	.8420	.4227
10	-41.87	319.1	-13.46	28.04	-4.994	8.121	-1.103	.7198	.8347	.4109
0	-52.32	402.5	-15.19	33.01	-6.004	10.27	-1.446	1.051	.8277	.3812
-10	-59.97	470.5	-17.20	38.95	-7.210	13.35	-1.847	1.536	.8305	.3817

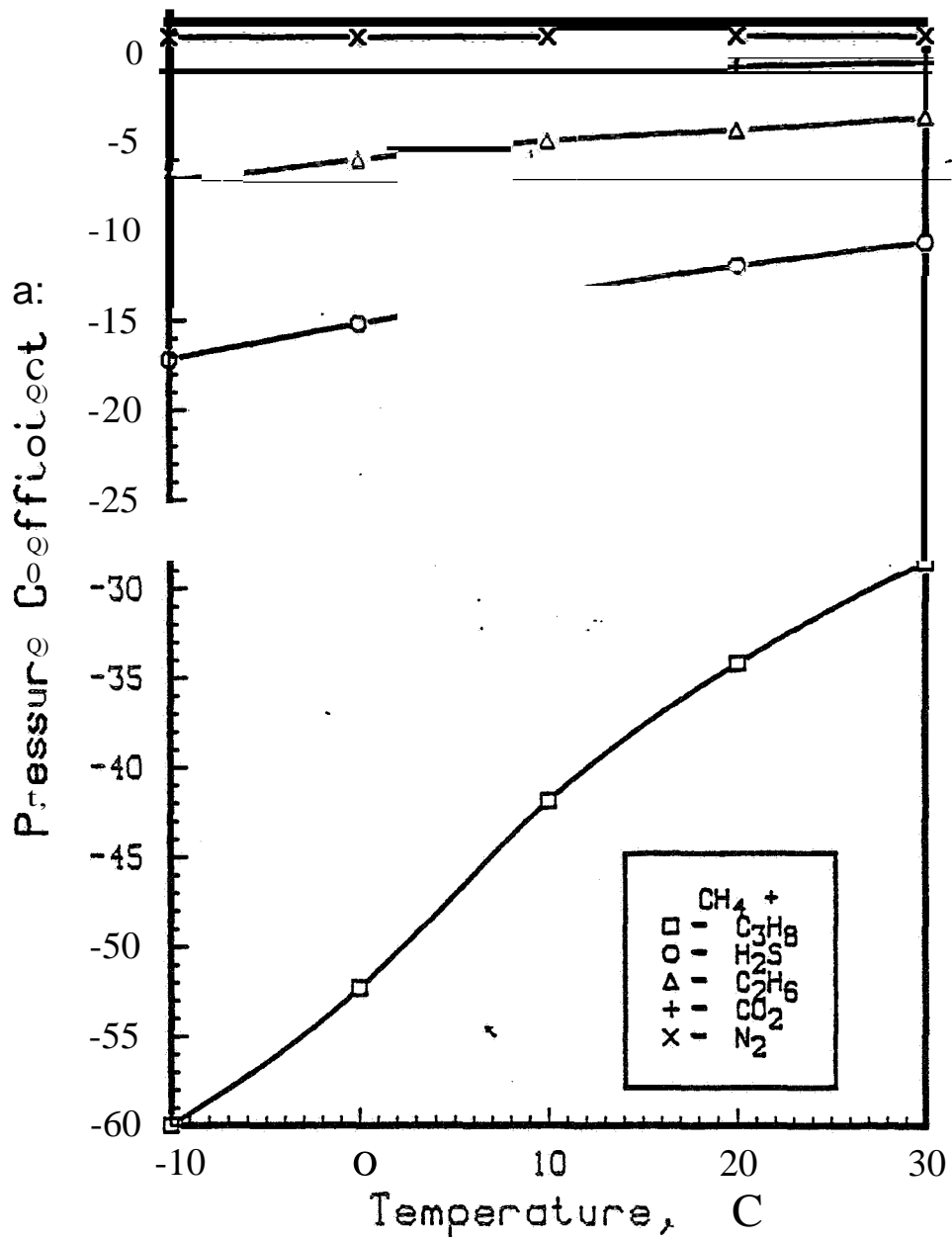


Figure 12: Temperature Dependence of Dissociation Pressure Coefficient, A.

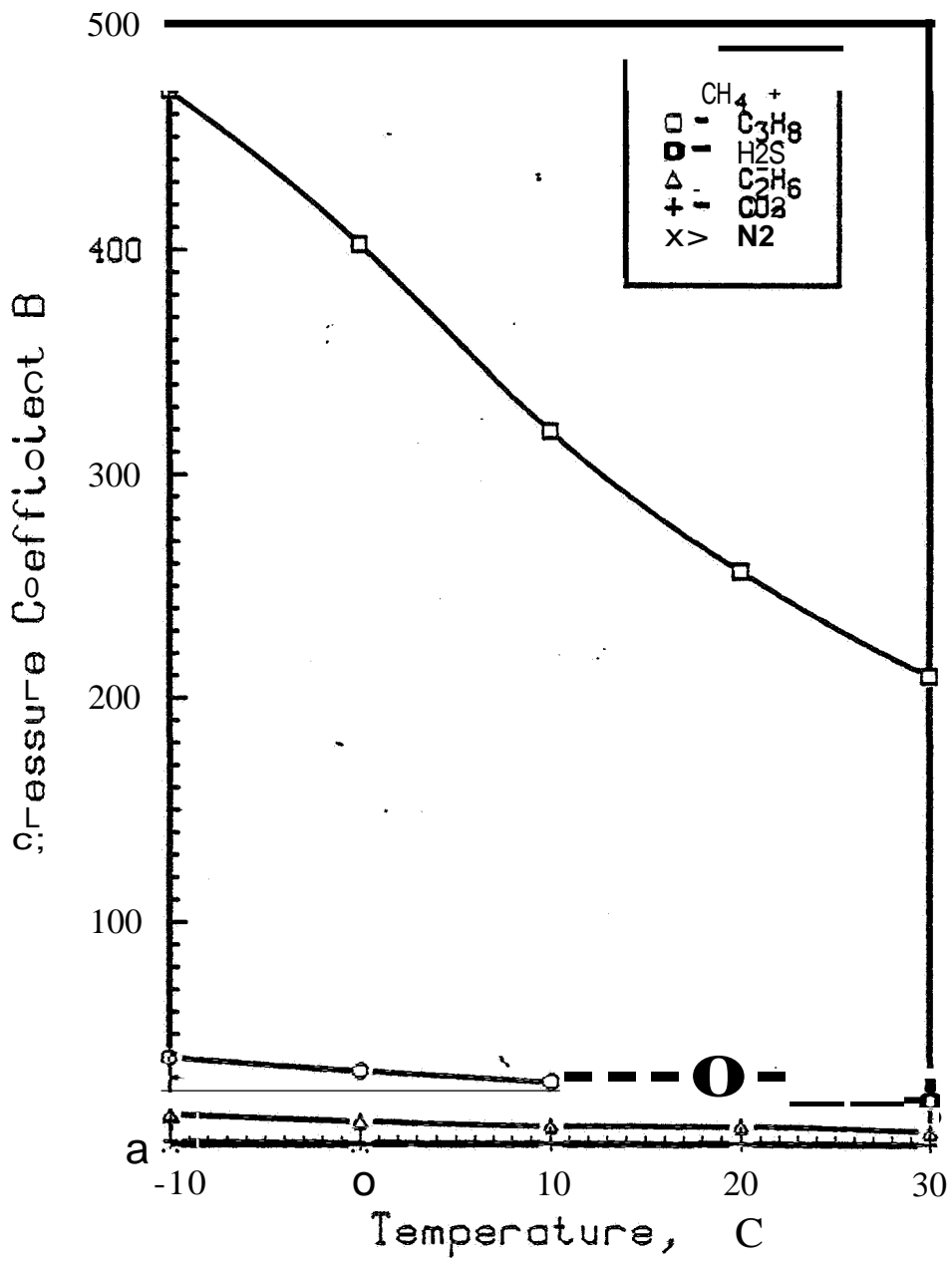


Figure 13: Temperature Dependence of Dissociation Pressure Coefficient, B.

5. Enthalpies of Hydrate Formation

The enthalpies of formation are calculated from the above dissociation pressure curves. The fundamental equation relating enthalpy of dissociation H_v , to equilibrium dissociation pressure, P , is

$$H_v = T \Delta V \frac{dP}{dT} \quad (\text{Clapeyron Equation}) \quad (5-1)$$

where ΔV is change in volume due to hydrate formation. This can be modified to

$$R_v = RT^2 \frac{d \ln P}{dT} - n \Delta V_w T \frac{dP}{dT} \quad (5-2)$$

At low pressures ($P < 1000$ kPa) the second term on the right can be neglected. In equation (5-1), Z is the compressibility factor of the gas in equilibrium with the hydrate, R is the gas constant, ΔV_w (Table III) is the volume of one mole of hydrated water less the volume of one mole of liquid water ($T > 273$) or one mole of ice ($T < 273$) and n is the number of moles of water per mole of gas in the hydrate phase (hydrate number).

Table III: Volume Changes Upon Converting Water to Hydrate'

	STRUCTURE	$T < 273.15K$	$T > 273.15K$	Units
ΔV_w	I	3.0	4.6	$\text{cm}^3/\text{gmol-water}$
ΔV_w	II	3.4	5.0	

The enthalpy change given in equation 5-2. is the amount of energy required to dissociate one mole of gas from the hydrate phase, leaving gas and water (or ice if $T < 0^{\circ}\text{C}$).

Enthalpies are given in Table IV. All slopes used to calculate the data in this table are based upon the data in Table I.

Table IV:- Dissociation Enthalpies of Pure Species

$$H_v \text{ (Cal/gmole)} = \underline{c} + \underline{dT} \quad T \text{ in } \underline{\text{kelvins}} \text{ -----}$$

GAS	e	d	Temp. range
	6533.8098	-11.9718	-25 to 0oC
	13520.842	-4.0247	0 to 25°C
	8457.57	-9.5926	-25 to 0oC
	13253.945	15.0017	0 to 14°C
	7608.6061	-4.9023	-25 to 0oC
	-37751.89	250.092	0 to 5°C
	9290.2084	-12.9276	-25 to 00C
	19198.7.53	-14.9547	0 to HOC
	4934.24	-9.0404	-25 to 00C
	6187.8015	18.3729	0 to 25°C
	8487.6168	-7.8068	-25 to 00C
	6781.8839	31.454	0 to 25°C

For gas mixtures, the effect of composition on enthalpy is shown in Figures 14-21*. Coefficients for determining the effect of composition are given in Table V. For gas mixtures the enthalpy regressions are

$$\ln (H_v/H_o) = \sum [A_i x_i + B_i x_i^2] \quad (5-3)$$

where the x_i are the mole fractions of the non-methane component and H_o and H_v are the dissociation enthalpies of methane and the gas mixture respectively. Figures 22 and 23 show the temperature dependence of these coefficients, and can be used for interpolation.

*Figures 14-21 show the energy required to convert hydrate to ice and gas at $T \leq 00C$ and to water and gas at $T > 00C$.

CH₄/C₂H₆ Gas Hydrates

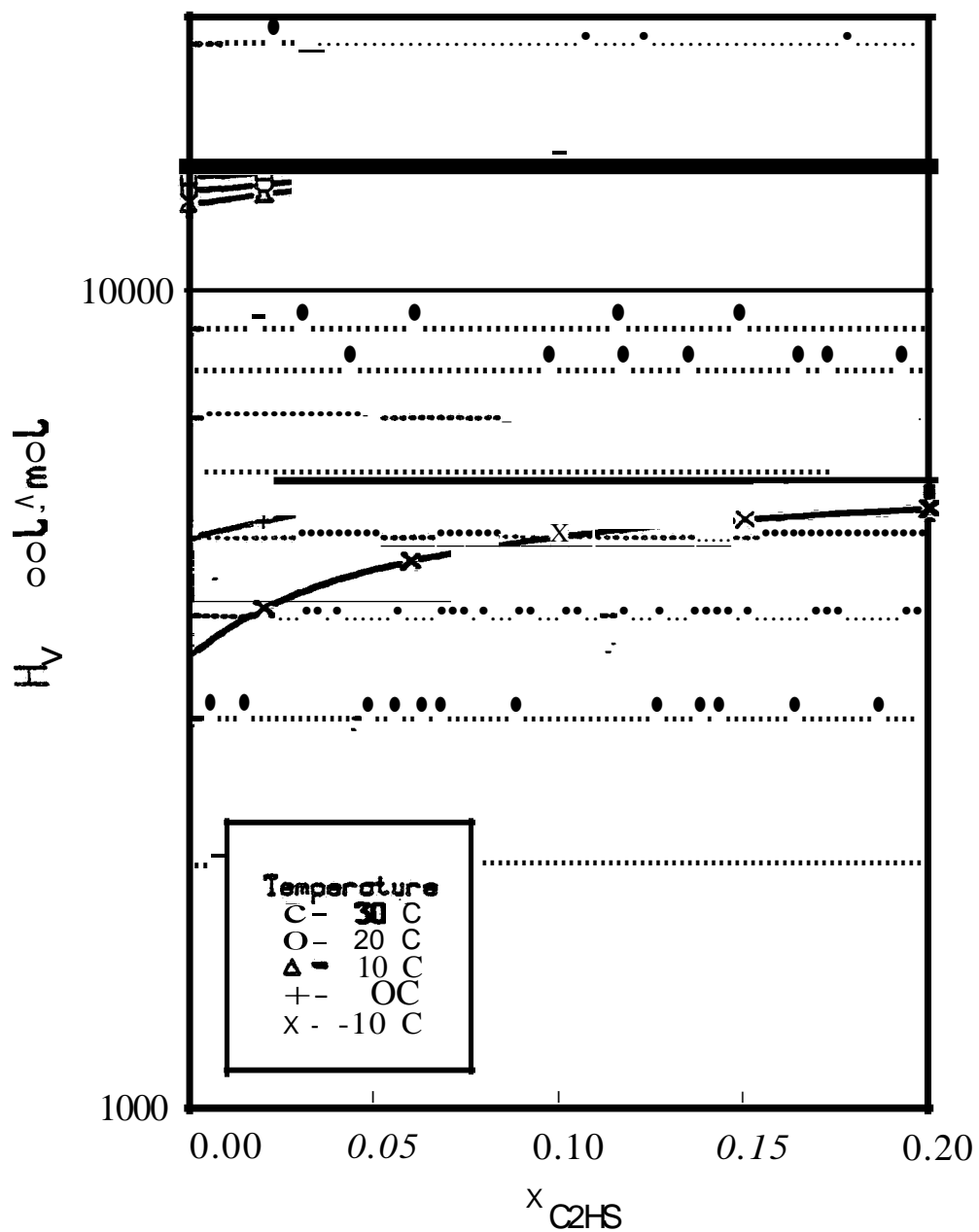


Figure 14: The Effect of Ethane on the Hydrate Dissociation Enthalpy in a Methane-Rich Gas

CH₄/CO₂ Gas Hydrates

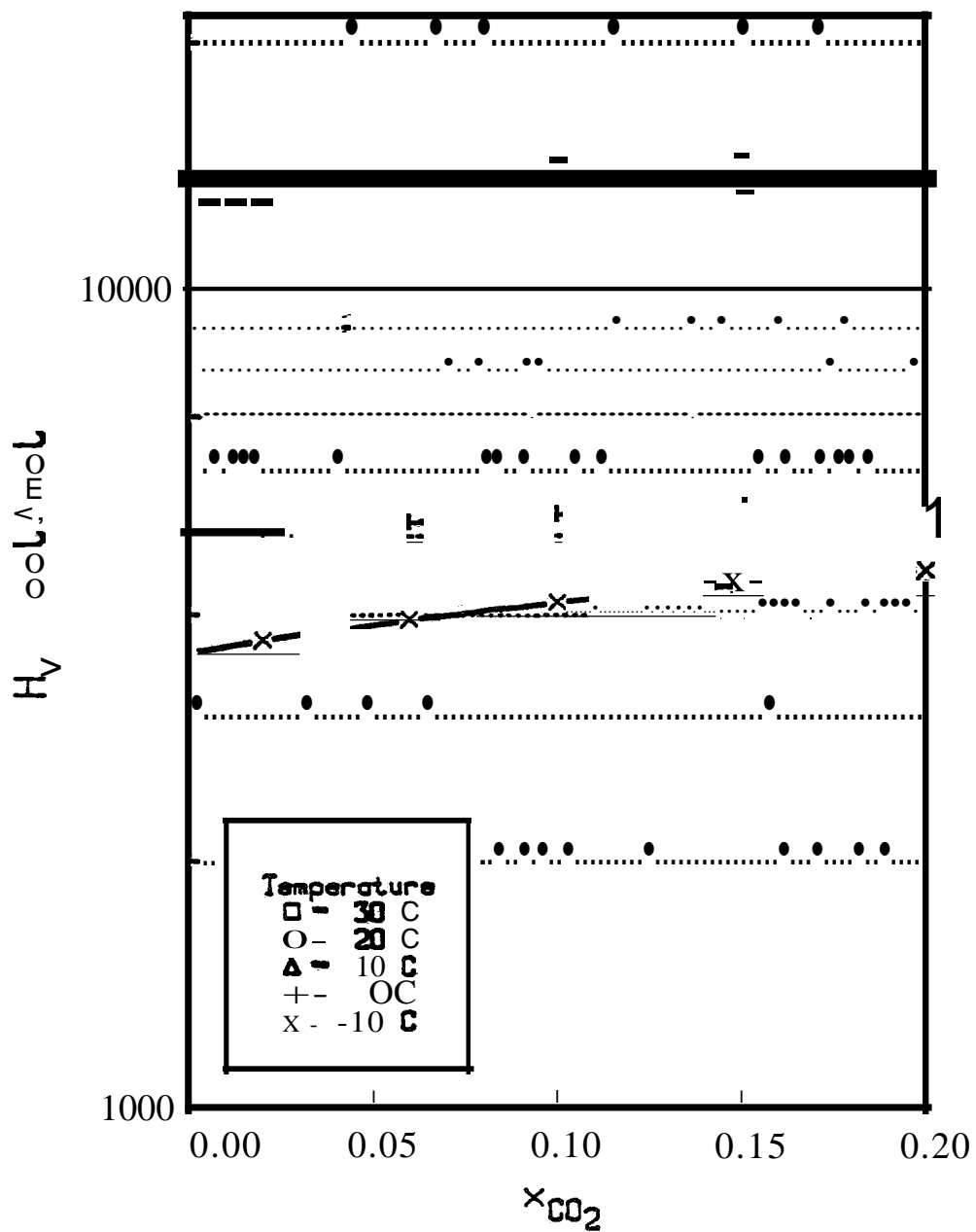


Figure 15: The Effect of Carbon Dioxide on the Hydrate Dissociation Enthalpy in a Methane-Rich Gas

CH₄/H₂S Gas Hydrates

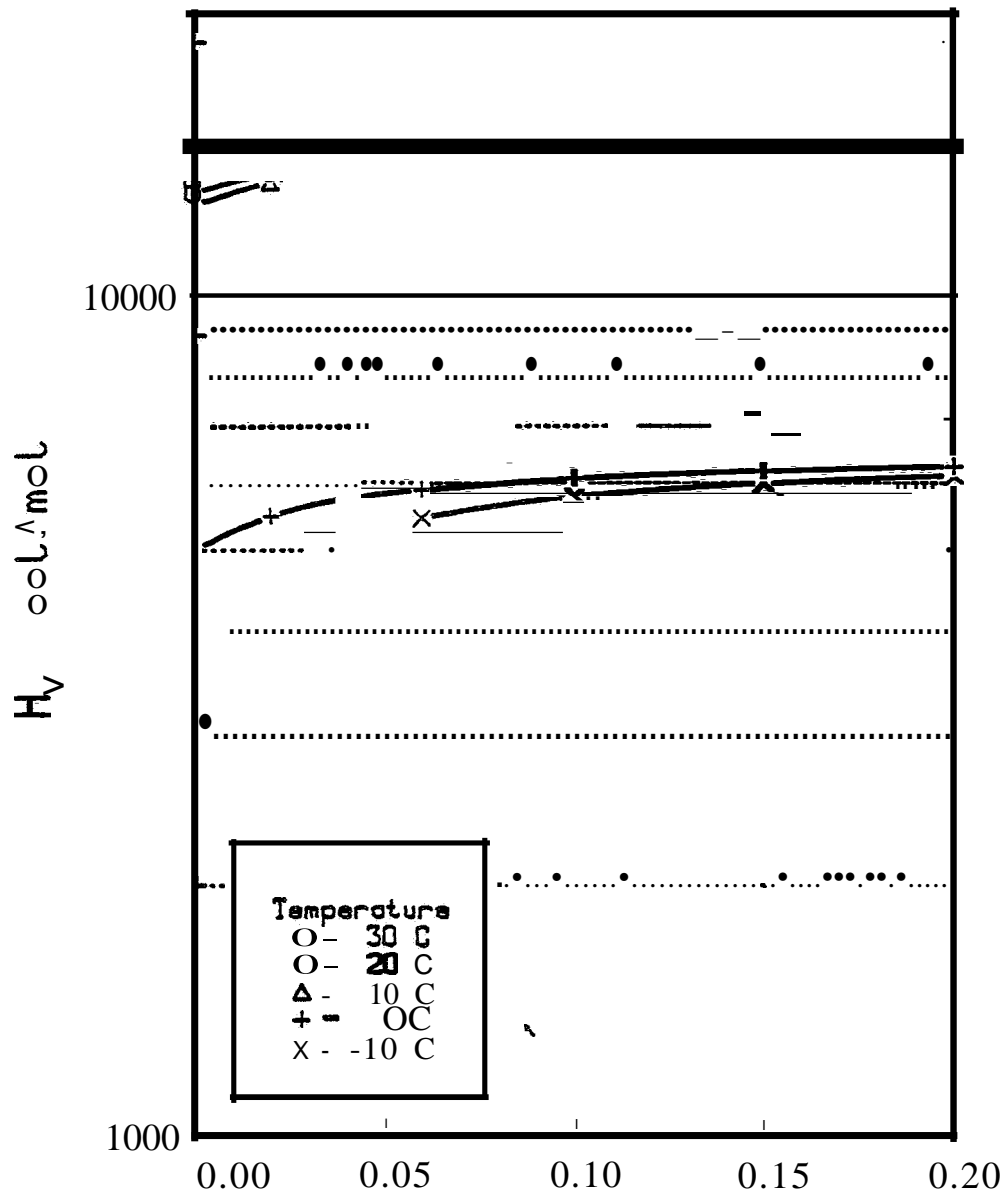


Figure 16: The **Effect** of Hydrogen Sulfide on the Hydrate Dissociation Pressure of a Methane-Rich Gas

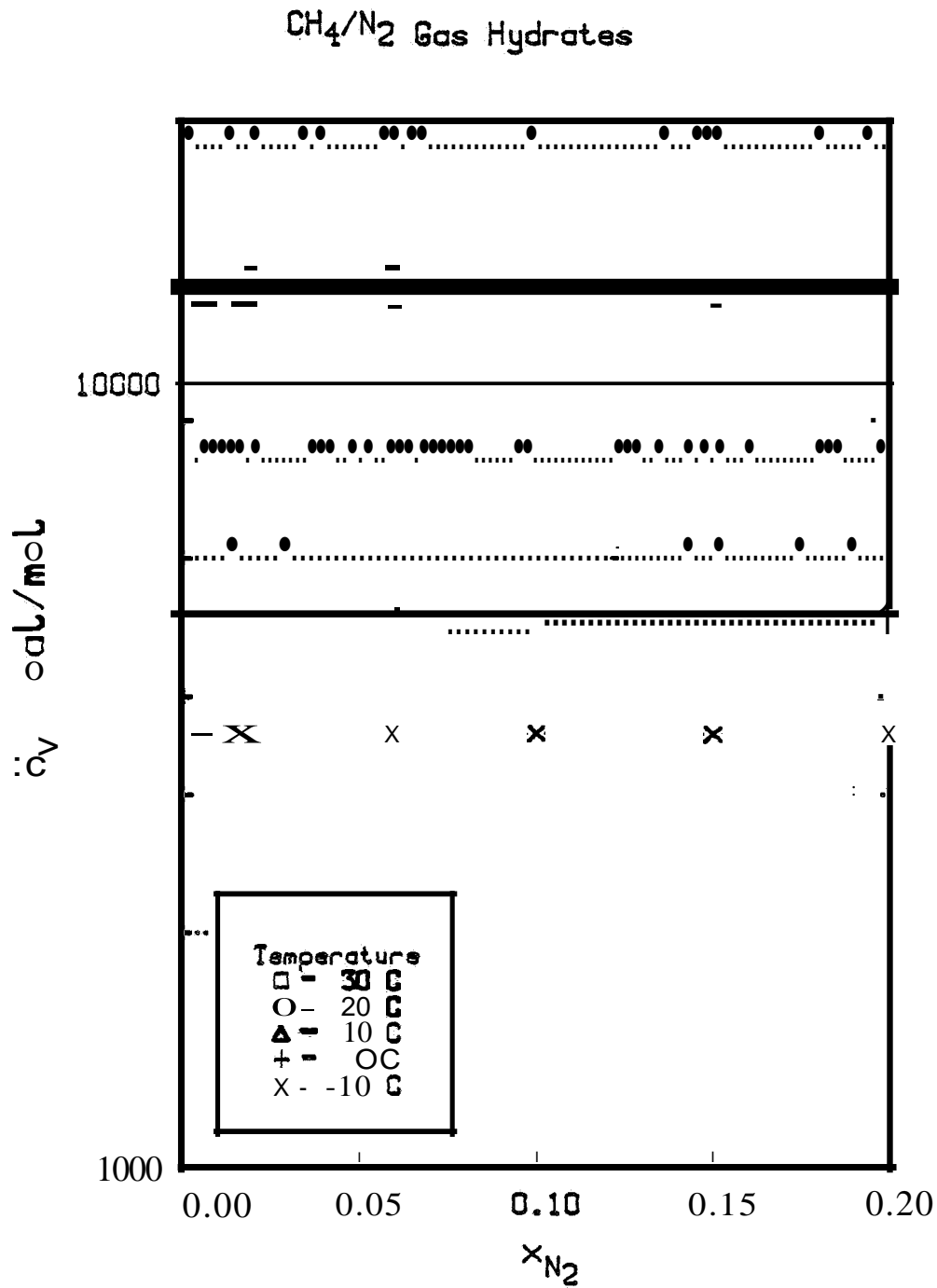


Figure 17: The Effect of Nitrogen on the Hydrate Dissociation Enthalpy in a Methane-Rich Gas.

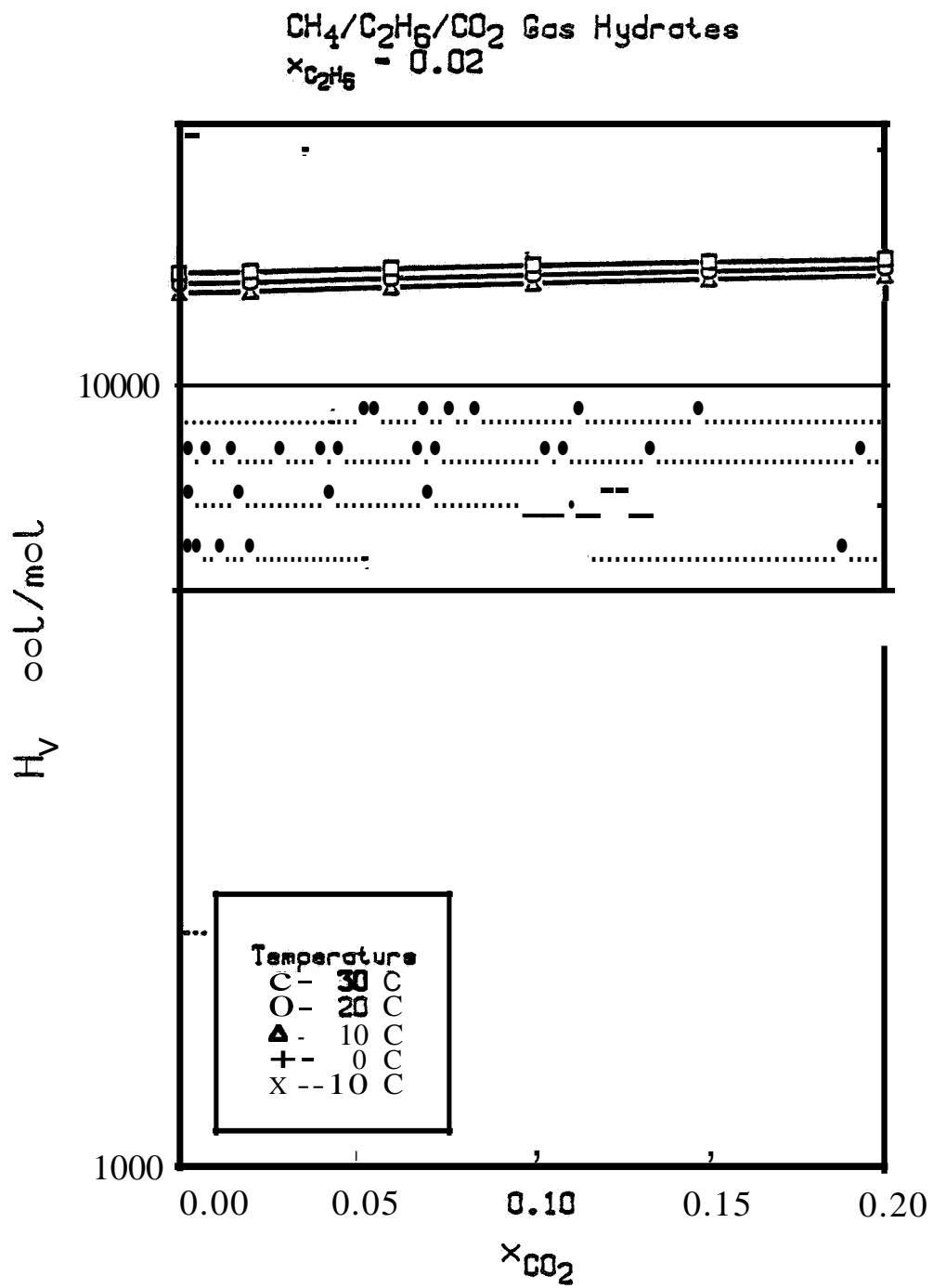


Figure 18: The Effect of Carbon Dioxide on the Hydrate Dissociation Enthalpy of a Methane + Ethane Mixture

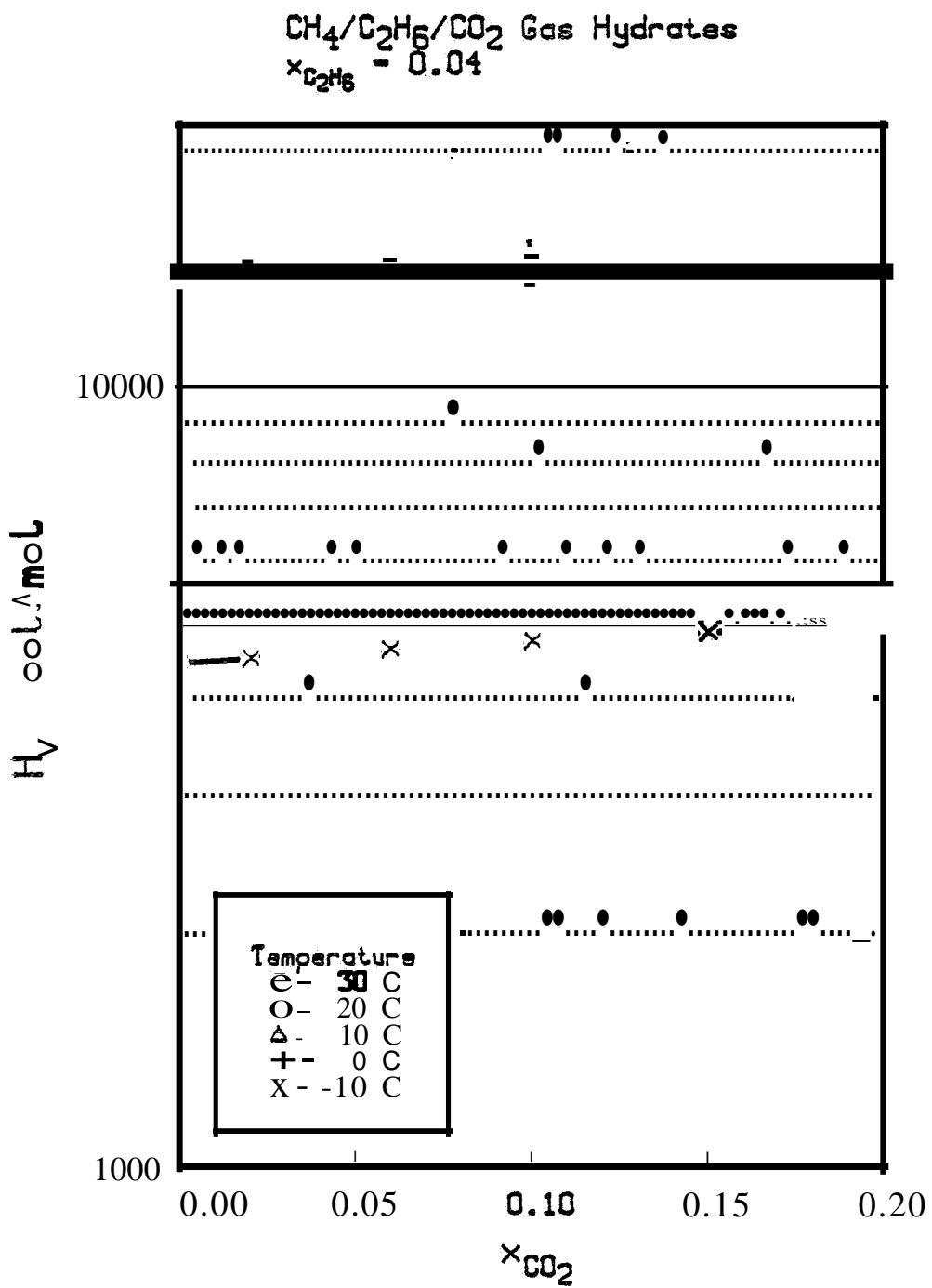


Figure 19: The Effect of Carbon Dioxide on the Hydrate Dissociation Enthalpy of a Methane + Ethane Mixture

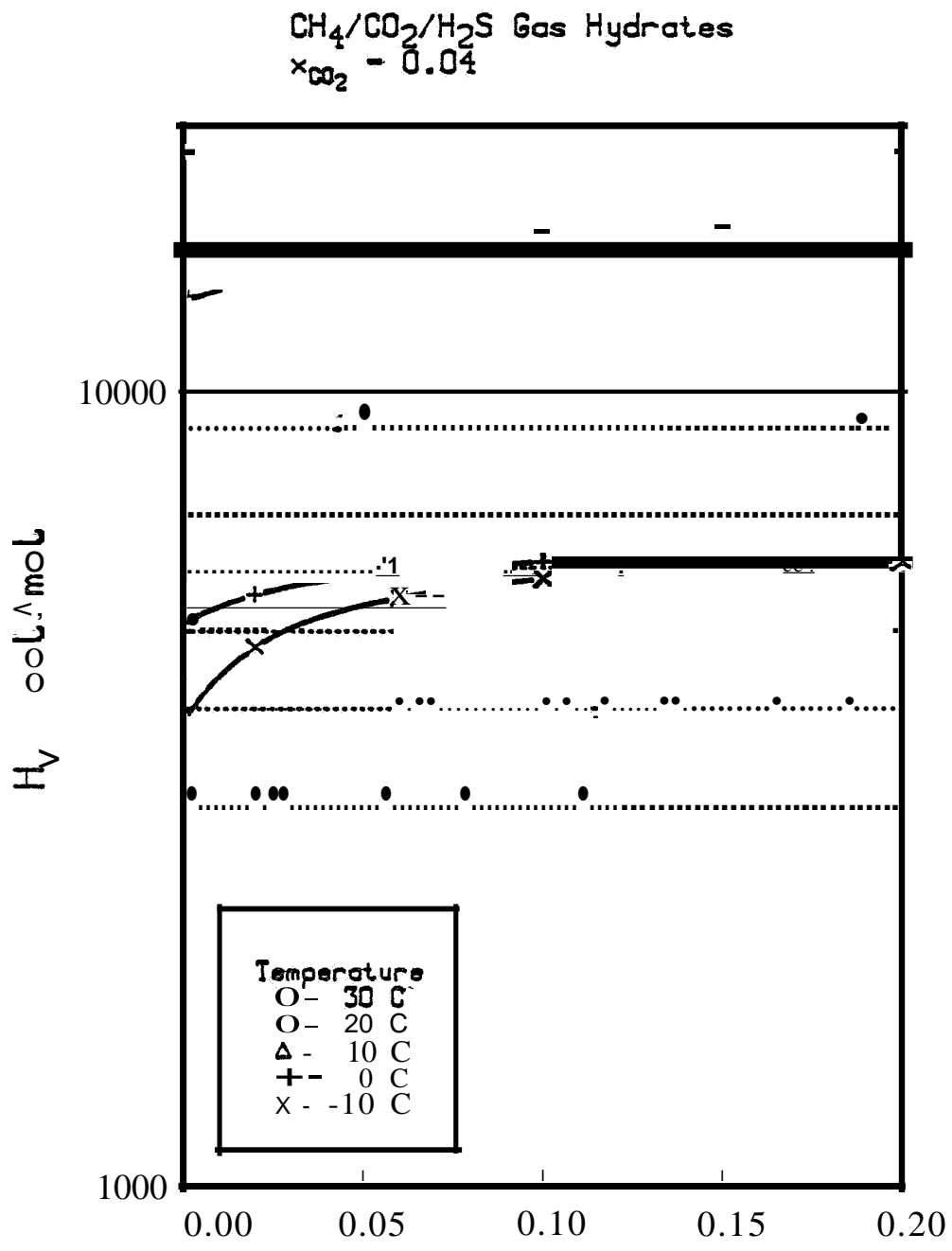


Figure 20: The Effect of Hydrogen Sulfide on the Hydrate Dissociation Enthalpy of a Methane + Carbon Dioxide Mixture

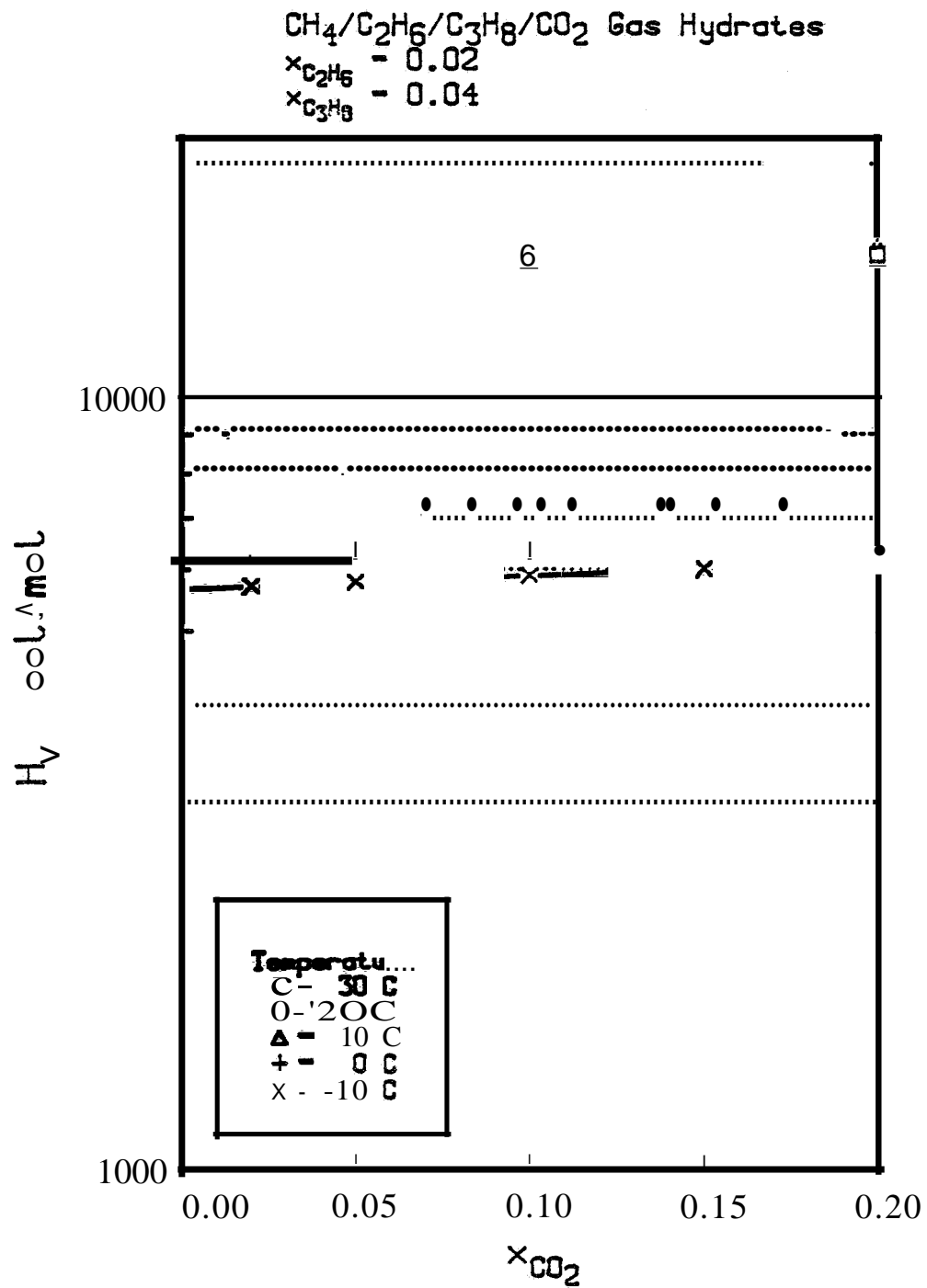


Figure 21: The Effect of Carbon Dioxide on the Hydrate Dissociation Enthalpy in a Methane + Ethane + Propane Mixture

Table V: **Coefficients** for Calculating the **Effect** of Other **Cases** on Dissociation **Enthalpies**

TOe	C ₃ H ₈		H ₂ S		C ₂ H ₆		CO ₂		N ₂	
	A	B	A	B	A	B	A	B	A	B
30	5.596	-44.62	1.651	-4.6Q3	.6105	-.9534	.2762	-.1914	.003207	-.01428
20	7.893	-65.01	1.851	-5.253	.9121	-1.833	.3270	-.2747	.001587	-.007836
10	10.20	-83.74	2.038	-5.891	1.164	-2.564	.3914	-.3891	-.002013	-.009398
0	12.45	-113.0	2.790	-8.238	1.858	-4.849	.6911	-.8484	+.2082	+.1750
-10	24.22	-217.4	6.903	-21.14	4.614	-12.70	1.728	-2.720	-.01794	-.009924

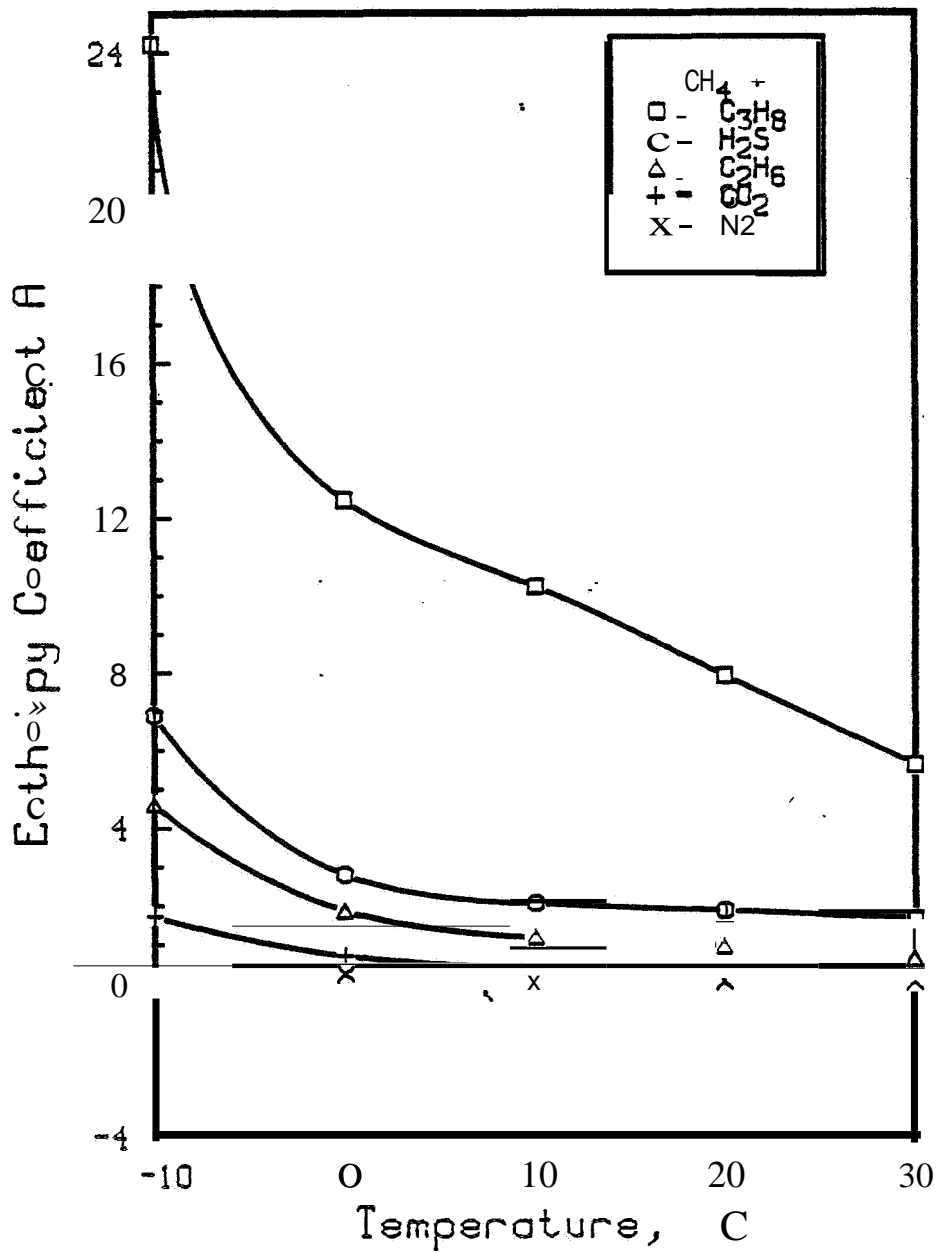


Figure 22: The Temperature Dependence of the Enthalpy Coefficient, A.

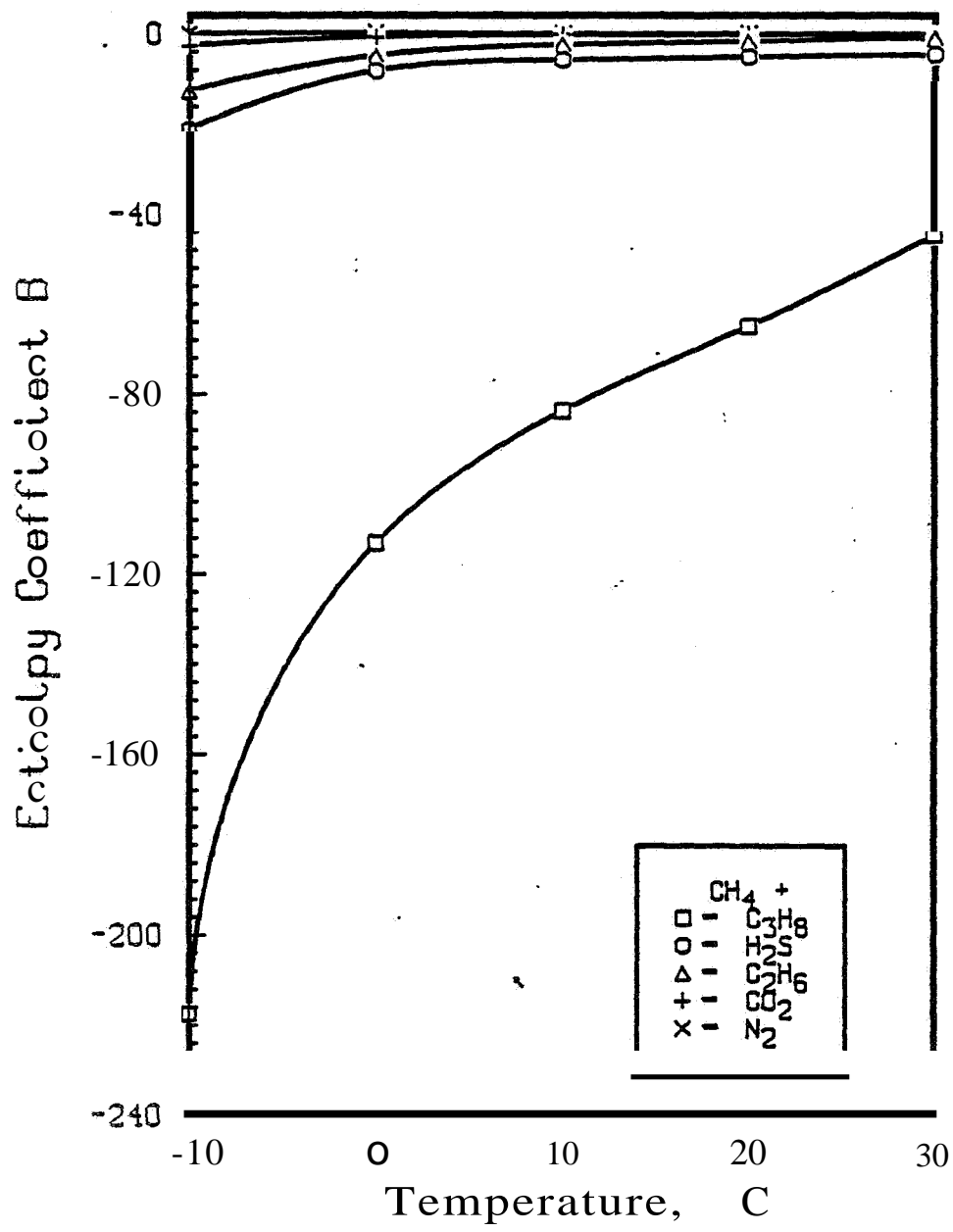


Figure 23: The Temperature Dependence of the Enthalpy Coefficient, B.

6. Heat Transfer Between Hydrates and a Warm Bulk Fluid

Very few studies have been reported in the literature about hydrate formation kinetics. Knox et al [18] investigated the kinetics of propane hydrate formation in a continuous stirred tank reactor. The rates of formation were quantitatively measured from the amount of hydrates formed. This study revealed that the yield of hydrates formed was function of contact time and the degree of subcooling. Barreret al [19,20] investigated kinetics of Ar, Kr and Xe hydrate formation. In these studies, hydrate formation was studied at very low temperatures. Makogon [1] investigated the kinetics of methane and ethane hydrate formation when a gas under pressure was bubbled through a stagnant liquid water. They developed an expression for the rate of nuclei formation in terms of the degree of subcooling below the equilibrium temperature. In most of these studies, no quantitative model was developed to predict the mass of hydrates formed as a function of time. Recently, Vysniauskas and Bishnoi [21] investigated systematically, the kinetics of methane hydrate formation. In their study, methane was contacted with continuously stirred water at constant pressure and constant temperature in a semi-batch stirred tank reactor. They reported that the rates of methane consumption (to form hydrates) were dependent on the interfacial area, pressure, temperature and the degree of subcooling. They developed a semi-empirical kinetic model to correlate the experimental data. However, the experiments in this study were performed at low conversions (10 percent of the water was converted to hydrates) and the influence of the conversion of water to hydrates on the rate of formation was not studied. The kinetic rate expression they presented also predicts a non-zero, finite rate when all the water is converted to hydrates which is obviously not correct.

Experimental

In the present study, the kinetics of methane hydrate formation was investigated. Figure 24 shows the schematic diagram of the experimental apparatus used to form hydrate cores. The pressure vessel used to form hydrates was made up of 316 stainless steel and had a removable flange at the top and a permanent flange at the bottom. This vessel had a capacity of 2.4 liters and was designed for pressures up to 13.8 MPa. This vessel was fitted with a gas inlet port and thermocouple ports and a Heise pressure gauge with a range of 0 to 2000 psia and with 2.5 psi divisions. The vessel was completely insulated to avoid heat exchange with surroundings. Pressure measurements were within ± 0.25 percent. Calibrated platinum resistance thermometers were used to measure the temperature of the gas and hydrate phases. The temperature ^{was} ~~were~~ controlled within ± 0.1 K by means of Extrol-150 temperature controller manufactured by Neslab Co. The accuracy of temperature measurement was ± 0.1 K.

A known quantity of frost (finely divided ice crystals) was charged to the vessel. The frost was compacted in such a way that a uniform cylindrical core of ice was formed to a required porosity.

The vessel was then sealed and evacuated to remove traces of air in the vessel. The frost was then contacted at 274K with methane at pressures between 6500 to 6900 KPa. Before pressurization with methane gas, the premature melting of frost was prevented. As hydrates were formed, the pressure in the vessel decreased. Formation of sufficient quantities of hydrate generally took between 60 and 220 hours. During the hydrate formation period, pressure and temperature were recorded as functions of time. From these data, the conversion of frost to hydrates ^{was} ~~were~~ obtained as a function of time. The hydrate number for methane, (the ratio of ^l ~~mols~~ of water to mols of

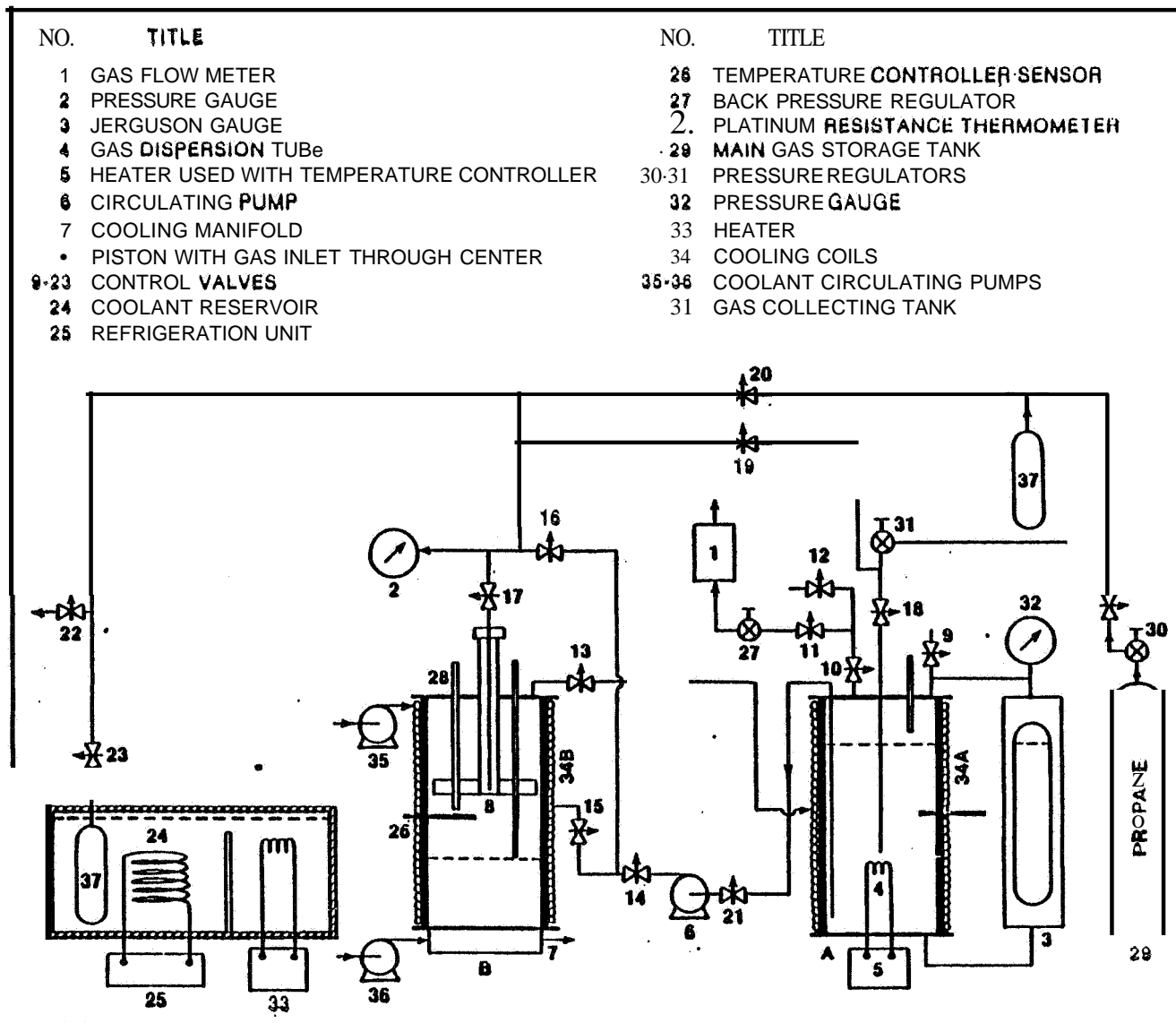


Figure 24: Experimental Apparatus

gas in the hydrate phase) was obtained from the final pressure data. The minimum value of the hydrate number obtained was 6.15 and was used in subsequent calculations of conversion.

Table VI gives the summary of different runs performed. Table VII gives the pressure-conversion time data for these runs.

Hydrate Formation Model

A model for formation of hydrates from ice is developed in this section. Consider an ice particle of spherical shape having an initial radius of R_0 . As gas is brought into contact with the ice, the hydrate formation takes place on the surface of the ice and hydrates form the outer layers. As time increases and hydrates form, the radius of the ice crystal, R , decreases. Assuming all ice particles are of the same size and shape, the mass of ice, H , can be related to the radius of each ice particle and the number of particles, N_p

$$M_0 = \frac{4}{3} \pi R_0^3 \rho N_p \quad (6-1)$$

$$M = \frac{4}{3} \pi R^3 \rho N_p \quad (6-2)$$

The surface area for hydrate formation can be given by the following relations

$$S_0 = 4\pi R_0^2 N_p \quad (6-3)$$

$$S = 4\pi R^2 N_p \quad (6-4)$$

Table VI

Summary of Hydrate Formation Runs

Run #	M ₀ (gms)	Hydrate Formation period (hra)	% Conversion of Frost to hydrates
1	504.1	66	90.3
2	482.0	66	75.2
3	515.1	68	86.6
4	492.5	89	90.0
5	501.9	141	89.5
6	466.0	221	100.0

Table VII

Pressure-Time-Conversion Data

Time (hrs)	P (KPa)	X
Run #1		
0	6626	0.000
18	5474	0.448
22	5288	0.492
31	4813	0.608
49	3785	0.850
66	3551	0.903
Run #2		
0	6736	0.000
1.25	6536	0.047
16.5	532.6	0.308
23	4944	0.390
41	3792	0.620
48.5	3468	0.685
66	3123	0.752
Run #3		
0	7074	0.000
2	6721	0.108
18	5205	0.433
25	4625	0.553
42	3395	0.800
48	3256	0.828
66	3067	0.863
68	3065	0.866
Run #4		
0	6809	0.000
3	6550	0.087
16.5	5654	0.369
25	5240	0.461
41.5	4502	0.623
65	3492	0.835
89	3179	0.900

Run #5

0	6914	0.000
3.25	6729	0.079
7.75	6311	0.196
29.75	5171	0.441
67.5	3506	0.799
77	3378	0.826
91.75	3213	0.860
100	3151	0.882
117.5	3068	0.889
141	3041	0.895

Run #6

0	7353	0.000
2	7315	0.095
17.5	6040	0.431
24	5750	0.503
45.5	4723	0.750
67	4254	0.861
89.5	4096	0.898
119	4020	0.916
138.75	3985	0.925
221	3978	1.000

The conversion of ice to hydrates is

$$x = \frac{M_o - M}{M} \quad (6-5)$$

The radius of an ice particle at any instance is given by

$$R = R_o (1-x)^{1/3} \quad (6-6)$$

The surface area, S, can be related to initial surface area, S_o by

$$S = S_o (1-x)^{2/3} \quad (6-7)$$

The rate of consumption of methane (moles/time/volume) is given by

$$r = \frac{M_o}{V_R M_w n} \frac{dx}{dt} \quad (6-8)$$

where, V_R is reactor volume, M_w is molecular weight of water and n is the ratio of mols of water to gas in the hydrate phase (6.15).

The following rate expression can now be written for the formation rate of hydrates,

$$r = K_S(C-C^*) \quad (6-9)$$

where, r is the rate of methane consumption in gmol per cm³ per hour, K is constant in (cm²/hr)⁻¹ and C is concentration of methane in the gas phase and C* is equilibrium concentration of methane. The concentrations C_o, C and C* are given by

$$C = \frac{P}{ZRT} \quad (6-10)$$

$$C^* = \frac{P^*}{Z^*RT} \quad (6-11)$$

$$C_0 = \frac{P_0}{Z_0RT} \quad (6-12)$$

From a material balance, we get

$$C - C^* = C_0 - C^* \frac{Mx}{V_R(Mw)n} \quad (6-13)$$

The superscript *, indicates an equilibrium value and the subscript 0 indicates an initial value at t=0.

From equations (6-8) to (6-13) we get

$$\frac{dx}{dt} = \frac{K V_R Mwn S_0}{M_0} (1-x)^{2/3} \left(\frac{P_0}{Z_0RT} - \frac{P^*}{Z^*RT} \frac{M_0 x}{V_R(Mw)n} \right) \quad (6-14)$$

This expression was numerically integrated and the lumped parameter KS_0 was obtained to fit the experimental data.

Figure 25 shows the comparison between experimental and predicted results.

Dissociation of Hydrates through Heat Transfer

The rate at which hydrates dissociate in a reservoir will be affected by the rate of heat transfer to the hydrate. There are two resistances to take into effect; these are the heat transfer resistance in the media surrounding the hydrate and the heat transfer resistance at the interface where the

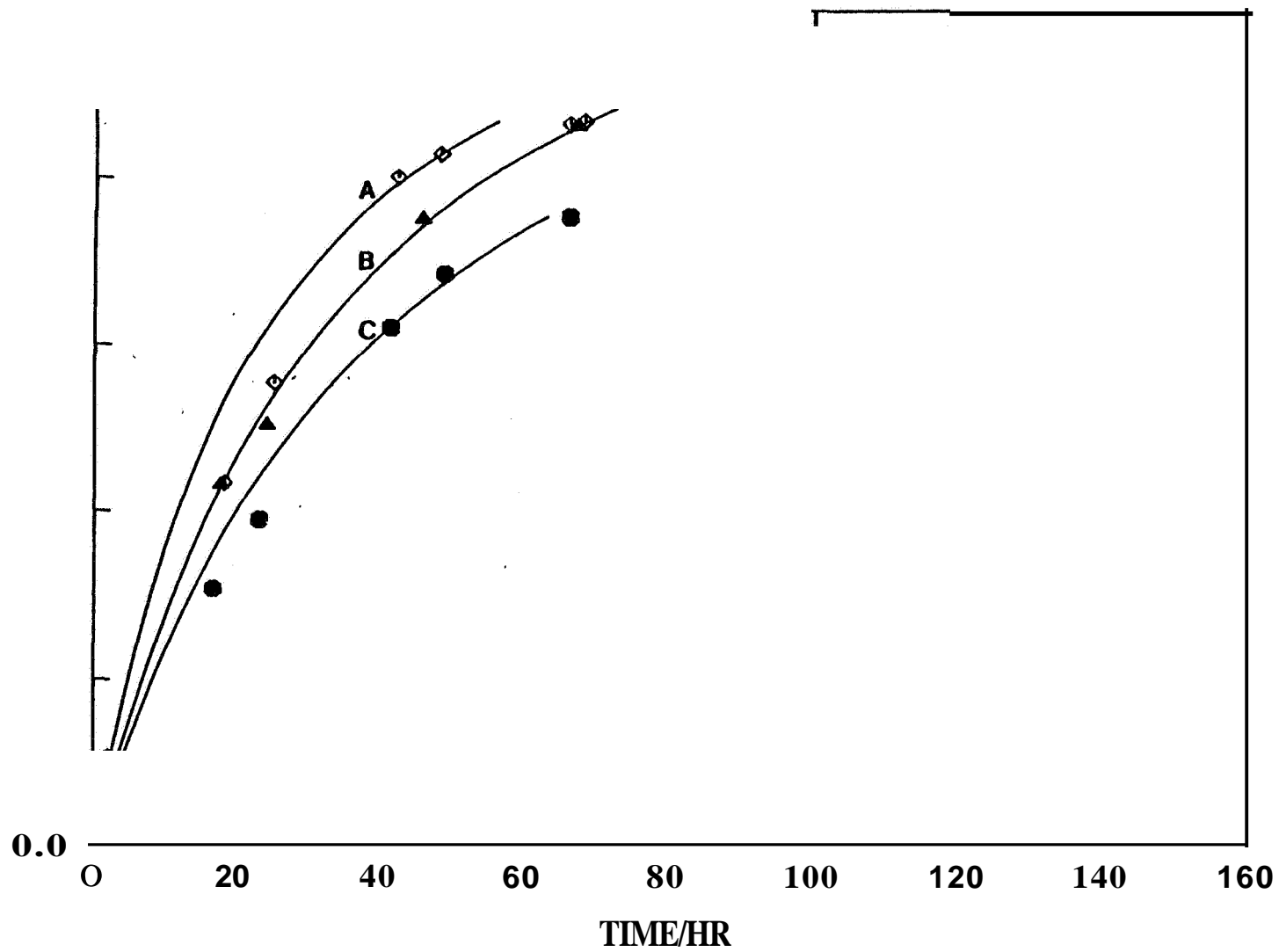


Figure 25: Comparison of Experimental (Points) and Predicted Conversions (Lines)

hydrates dissociate. In this report, the significance of these two resistances is illustrated and methods of obtaining them are quantified.

Consider a model as shown on Figure 26 where a circulating fluid is used to heat up a hydrate containing zone. Heat is transferred from the water to the hydrate. However as the hydrates dissociate they leave a zone containing water, rock(sand) and some gas. (The amount of gas present is considered to be negligible in this analysis.) This sand + water zone (SWZ) builds up as hydrates decompose and thus provide resistance to heat transfer. The following model is developed.

The heat transfer per unit area (Q/A) from-water to sand zone is given by

$$\frac{Q}{A} = k_{eff} \left(\frac{T_B - T_S}{h_S} \right) \quad (6-15)$$

T_B = Circulating water temperature.

T_S = Sand temperature at the sand-hydrate interface.

where k_{eff} is an effective thermal conductivity of the SWZ and h_S is the SWZ thickness. The heat transferred from sand zone to hydrates must be the same and is given by;

$$\frac{Q}{A} = h\Delta T = h(T_S - T_H) \quad (6-16)$$

Figures 27a and 27b show the heat flux (Q/A) and rate of dissociation, versus ΔT . These are the quantities which are important in heat transfer models. Heat transfer coefficients can be obtained by dividing (Q/A) by ΔT . (In Figure 27b, the rate of dissociation is per unit hydrate area, which is the total cross-sectional area times the hydrate volume fraction). The curves

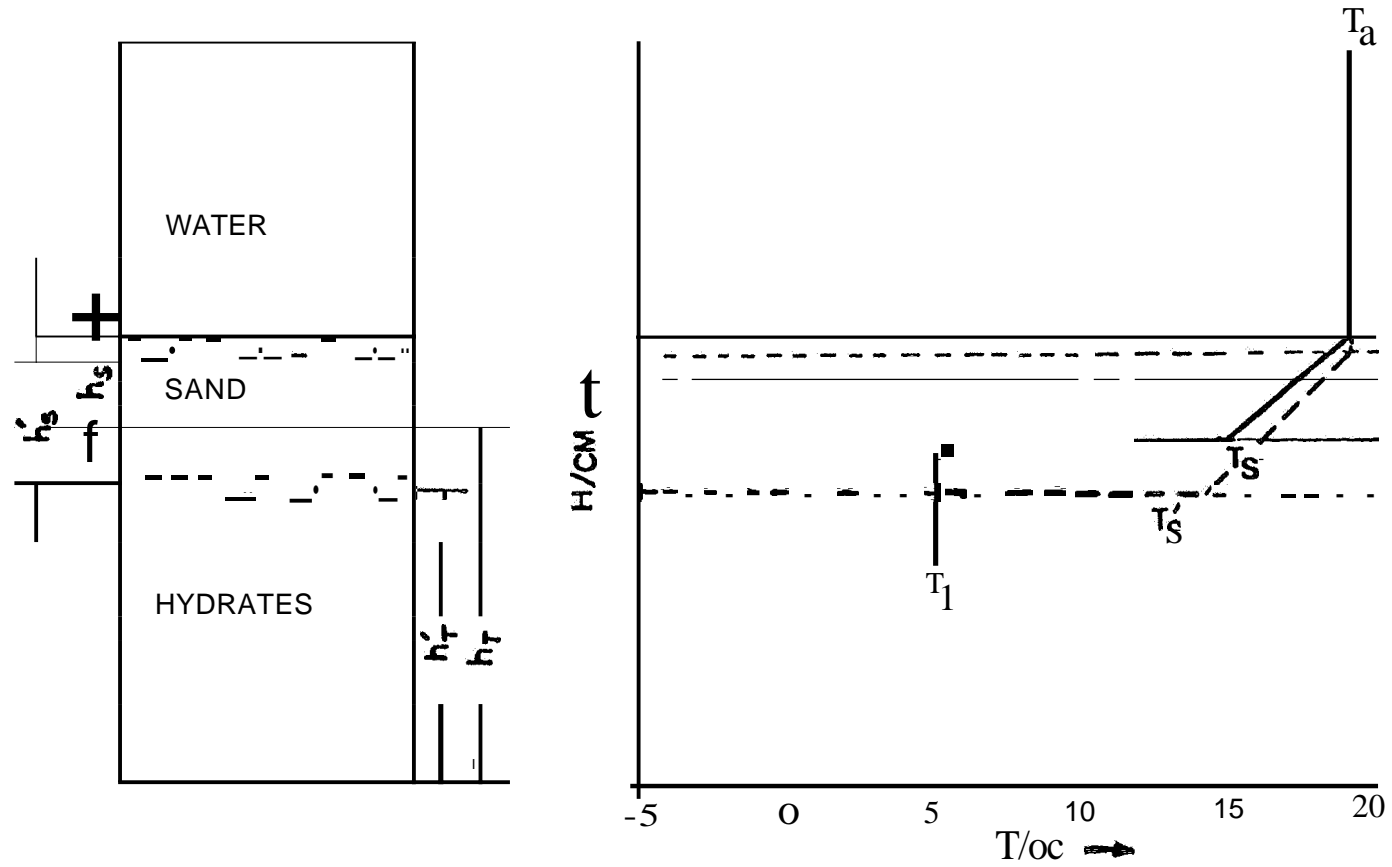


Figure 26: Schematic Diagram Representing Temperature Profile for Unsteady State Dissociation •

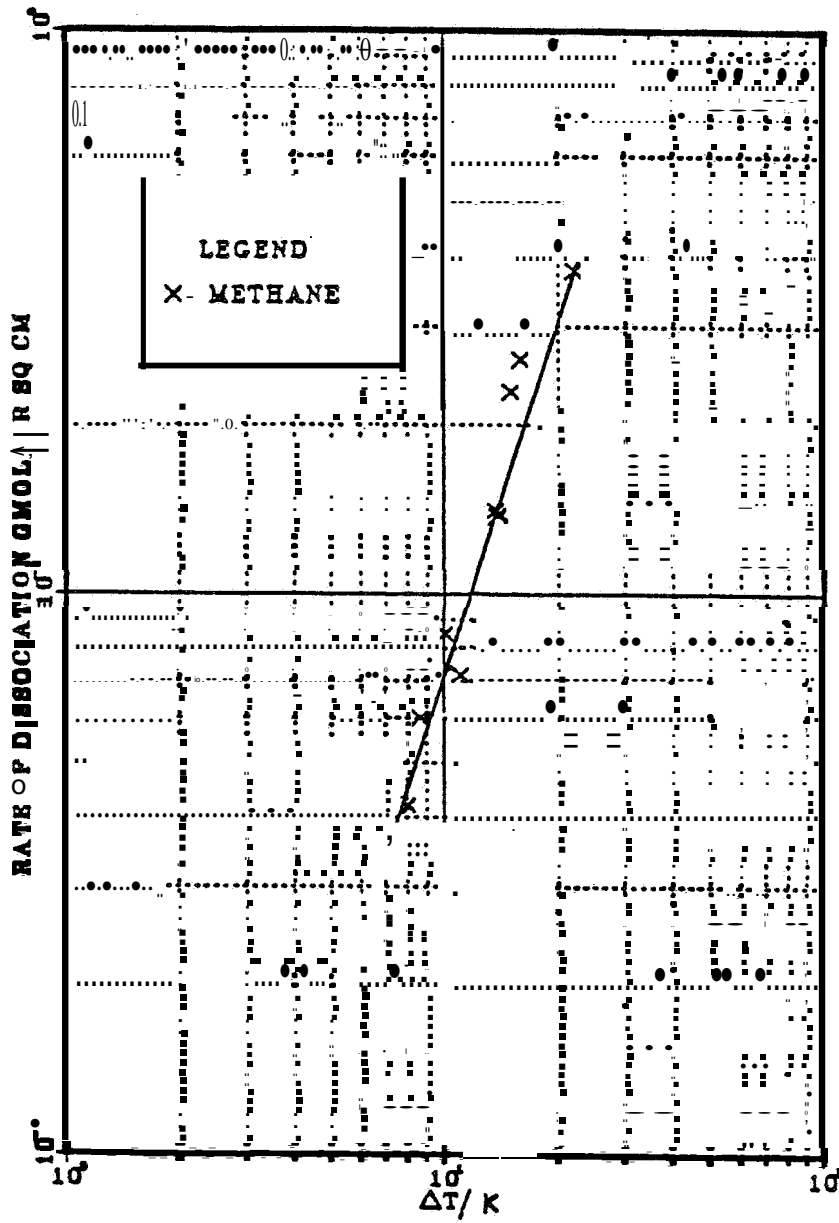


Figure 27b: Rate of Dissociation Versus Temperature Driving Force for Methane Hydrate Dissociation.

shown in these figures should not be extrapolated below 0°C for T_H or above $T_H=250C$. In equation (6-16) T_H is the hydrate equilibrium temperature at the reservoir pressure; and h is the three phase heat transfer coefficient at the sand-hydrate interface. It is a function of ΔT only. Combining these equations allows

$$K_{eff} \frac{(T_B - T_S)}{h_S} = h(T_S - T_H) \quad (6-17)$$

Initially, there is no sand zone. (This is not necessarily true, but the initial thickness is arbitrary so it is set to zero.) If the sand zone thickness is zero then $T_B = T_S$. Since $T_B \geq T_S \geq T_a$, the magnitude of ΔT and consequently the heat transfer are initially at their highest value where $t = Q$. As time increases, hydrates dissociate, the height of the SWZ, h_S , increases, and the heat transfer, Q/A , decreases.

The other limiting extreme is when the sand thickness gets very large. In this case T_S approaches T_a , since the resistance across the SWZ also becomes very large. Consequently the heat transfer and hydrate dissociation rate approach zero.

It is important that investigators be aware of these two extremes. All studies have ignored the resistance to heat transfer at the hydrate interface and most studies have ignored the resistance of the adjacent media (SWZ here). However, hydrates can only dissociate into gas when the necessary energy is transferred across the hydrate interface. For thermal stimulation, calculations of dissociation rates are based solely upon the rate of energy injection and as a result are too high. Even models based upon depressurization cannot hope to be realistic unless these resistances are accounted for.

To illustrate the importance of these resistances a case study has been prepared. Table VIII defines the variables used. This calculation is based upon a unit area of 71 cm^2 which is extremely small compared to the areal extent of a reservoir. Consequently, the absolute magnitudes of heat transfer and dissociation rates will be small. For an actual reservoir, the rate will increase, approximately, in proportion to the increase in hydrate cross sectional area. The affect of the sand thickness is absolute however, i.e. 2 cm of sand have the same effect in a reservoir as it does in the model.

Calculations:

1. Temperature of hydrates:

The hydrates are assumed to dissociate at an equilibrium temperature corresponding to the system pressure. Thus, the VL_{1H} curve for methane hydrates is used to obtain T_H .

The VL_{1H} curve for methane hydrates gives,

$$P/\text{kPa} = \exp\left(38.98 - \frac{8533.8}{T_H + 273.15}\right) \quad (6-13)$$

@P = 600 psia i.e. 4136.84 kPa

$T_H = 5.26^\circ\text{C}$

This temperature T_H remains constant throughout the dissociation.

2. Rate of Dissociation:

This is function of $(T_S - T_H)$ only and is determined by the heat transfer coefficients. Initially the rate of dissociation corresponds to a ΔT of $T_B - T_H = 30 - 5.26 = 24.74^\circ\text{C}$. This ΔT will be different if the temperature of thermal fluid (water) is different than 30°C or if the pressure is different than 4137kPa which implies $T_a=5.26^\circ\text{C}$. The equation

Table VIrI Variables for Case Study

h_{Ti} = Initial height of the hydrate zone.

h_{Si} = Initial height of the sand zone = 0

h_T = Height of the hydrate zone at time t, cm.

h_S = Height of the sand zone at time t, em.

A = Cross sectional area = 70.885 cm².

p = Pressure at which dissociation is occurring = 600 psia.

= Temperature of bulk water phase which is constant throughout the dissociation period = 30°C.

ϕ_H = Volume fraction of hydrates in the core = 0.5 •

ϕ_S = Volume fraction of sand in the hydrate core = 0.1 •

ϕ_G = Volume fraction of gas in the hydrate core = 0.4 •

V = Volume of the vessel = 2000 cm³ •

$\phi_{S'}$ = 0.527 •

below is based upon experimental data of hydrate dissociation by hot water. Data were obtained at the University of Pittsburgh.

$$\begin{aligned} \dot{m}_{H_2O} &= \frac{\text{gmole methane liberated}}{\text{hr. cm}^2 \text{ (hydrate area)}} \\ &= 6.155 \times 10^{-4} (T_S - T_H)^{2.186} \quad [\text{from experimental data}] \quad (6-19) \\ &= 6.155 \times 10^{-4} (24.74)^{2.186} \\ &= 0.6842 \text{ gmole CH}_4 / \text{hr. cm}^2 \text{ hydrate} \end{aligned}$$

$$\text{cm}^2 \text{ hydrate} \cdot A\phi_H = 70.85 \times 0.5 = 35.4425 \text{ cm}^2$$

$$\begin{aligned} \dot{m}_{H_2O} &= \text{initial rate of methane liberation at } t=0 \\ &= \frac{0.6842 \times 35.4425}{60} = 0.4042 \text{ g mole methane} \\ &\quad \text{min} \end{aligned}$$

3. Instantaneous Rate of Dissociation \dot{m}_H ($\frac{\text{gllol CH}_4}{\text{min}}$) at t)0

$$\dot{m}_H = 3.6358 \times 10^{-4} (T_S - 5.26)^{2.186} \quad (6-20)$$

4. Instaneous Height of the hydrate zone h_t

$$\dot{m}_H \frac{1}{A} \frac{d[ht]}{dt} = \dot{m}_H \quad (6-21)$$

where: n_H is 6.15 gmol water/gmol CH₄
 ϕ_H is 0.5 cm³ hydrate/cm³
 A is 70.885 cm²
 h_T is in cm
 $\rho_{H_2O, H}$ is 0.044 gmol water/cm³ hydrate

for this case,

$$-\frac{dh_T}{dt} = 3.944 \dot{m}_H \quad (6-22)$$

5. Instantaneous sand thickness. h_s

$$\frac{(h_{T_i} - h_T) \phi_s A}{\phi_s' A} = h_s$$

$$\text{or } h_s = 0.19 [h_{T_i} - h_T] \quad (6-23)$$

We know that, \dot{m}_H , T_S , h_s , h_T , h , $\frac{Q}{A}$ are functions of time.

6. Initially

$$\dot{m}_H = \dot{m}_{H0} = 0.4042 \text{ gmol CH}_4/\text{min}$$

$$T_S = T_{B''} = 30^{0C}$$

$$h_s = 0$$

$$h_T = h_{T_i}$$

7. Calculation of Effective Thermal Conductivity:

Assume that K_{eff} is constant.

Using Glandt's paper [22]:

k_w = thermal conductivity of water

$$= 0.5163 \text{ kcal/hr m k}$$

k_s = thermal conductivity of sand:

$$.. 0.2828 \text{ Kcal/hr m k}$$

$$\phi_s = 0.527$$

$$\alpha = \frac{k_s}{k_w} .. \frac{0.2828}{0.5163} .. 0.5477$$

$$A = \frac{1}{4} \left[3\phi_s' - 1 + \frac{(2-3\phi_s)}{\alpha} \right] .. 0.3365$$

$$K_{eff} = k_w \left[\alpha A + \left(\alpha^2 A^2 + \frac{\alpha}{2} \right)^{1/2} \right]$$

$$K_{eff} .. 0.3816 \text{ Kcal/hr .mK}$$

8. Calculation of heat of dissociation, ΔH_D

$$\Delta H_D \left(\frac{\text{Cal}}{\text{gmol methane}} \right) .. 13520.84 - 40247(T_{H+273} \cdot 15) \quad (6-24)$$

$$@T_H = 5.26^\circ\text{C}$$

$$\Delta H_D .. 12.4 \text{ Kcal/gmol CH}_4$$

9. Heat Transfer Coefficient for Methane Hydrates

$$h = \frac{60 \dot{m}_H \Delta H_D \times 10^4}{A (T_S - T_H)} \quad (6-25)$$

Using equations (6-20 and (6-24) we get:

$$h = 38.161(T_s - 5.26)^{1.186} \quad (6-26)$$

h is in Kcal/m²-hr-K

10. Obtaining T_s as Function of Time:

Using equation (6-17):

$$\frac{0.3816}{s} \frac{(30-T_s)}{h} \times 100 = 38.161 (T_{s-5.26})^{2.186}$$

$$\text{or } \frac{(30-T_s)}{h} = (T_{s-5.26})^{2.186} \quad (6-27)$$

Now from (6-20), (6-22), and (6-23) we get:

$$\begin{aligned} \frac{dh_s}{dt} &= -0.19 \frac{dh_T}{dt} \\ &= 0.19 \times 3.944 \dot{m}_H \end{aligned}$$

$$\frac{dh_s}{dt} = 2.72245 \times 10^{-4} (T_s - 5.26)^{2.186} \quad (6-28)$$

Using equation (6-27):

$$\begin{aligned} \frac{(30-T_s)}{(T_s-5.26)^{2.186}} &= h_s \\ \text{or } \frac{dh_s}{dt} &= \frac{d}{dt} \left[\frac{(30-T_s)}{(T_s-5.26)^{2.186}} \right] \quad (6-29) \end{aligned}$$

From 28 and 29 we get:"

$$\frac{d}{dt} \left[\frac{(30-T_S)}{(T_S-5.26)^{2.186}} \right] = 2.724 \times 10^{-4} (T_S-5.26)^{2.186} \quad (6-30)$$

This is differential equation in T_S and can be solved to obtain T_S as function of time.

$$\frac{dT_S}{dt} = 2.2972 \times 10^{-4} \frac{(T_S-5.26)^{5.372}}{(T_S-50.86)}$$

Integrating from $t=0$

$$\text{and } T_S = 30$$

we get:

$$\int_{30}^{T_S} \frac{(T_S - 50.86)}{(T_S - 5.26)^{5.372}} (dT_S) = \int_0^t 2.2972 \times 10^{-4} dt$$

Define $T_S' = T_S - 5.26$ gives:

$$\frac{10.43}{T_S' 4.372} \frac{0.2966}{T_S' 3.372} = 2.2972 \times 10^{-4} t + 2.4622 \times 10^{-6}$$

SUMMARY OF EQUATIONS REQUIRED

$$\frac{10.43}{(T_S - 5.26)^{4.372}} - \frac{0.2966}{(T_S - 5.26)^{3.772}} = 2.2972 \times 10^{-4} t + 2.4622 \times 10^{-6} \quad (6-31)$$

$$\dot{m}_H = 3.6358 \times 10^{-4} (T_S - 5.26)^{2.186} \quad (6-32)$$

$$h = 38.161 (T_S - 5.26)^{1.186} \quad (6-33)$$

$$h_s = \frac{(30 - T_S)}{(T_S - 5.26)^{2.186}} \quad (6-34)$$

$$h_T = h_{T1} - 5.2632 h_s \quad (6-35)$$

$$\frac{Q}{A} = 38.161 (T_S - 5.26)^{2.186} \quad (6-36)$$

These equations can be combined to solve for the various parameters of which the dissociation rate is of most interest. Mathematically it is more convenient to treat T_S as the independent variable. Results are shown on Figure 28.

From the results, it is clear that the dissociation rate drops off drastically as the thickness of the sand zone increases. In general models have assumed that the dissociation rate is infinite, that any energy injected will instantaneous be used to convert hydrates to gas and water. Recent experiments have shown that the calculated effective thermal conductivity may be 4 to 8 times calculated low so that the dissociation rate would be higher than Figure 28 indicates by factor of 4 to 8. Note that even the low dissociation rates, say 0.01 gmoles of CH_4/min , correspond to very high

production rates. A rate of 0.001 gmoles/min. corresponds to 32.2 liters/day and this is only for a heated contact area of 71 cm². Each square meter of heated area could produce 4,500 liters/day (about 160 ft³/day). By extrapolation, a heated area of 6,000 square meters (77 meters squared) would produce 1,000,000 SCFD of methane from hydrate. Table IX identifies some production rates for various conditions. These rates only indicate how hydrate dissociation is affected by 1) a layer of media (sand in this case) between the hot injection fluid (30°C) and the cold dissociating hydrate and 2) the interfacial resistance to heat transfer across the hydrate interface.

Table IX: Dissociation of Methane Hydrates; Examples

Case I		Case II	
ϕ_H	= 0.15	ϕ_H	= 0.50
ϕ_B	0.85	ϕ_B	= 0.10
T_B	31°C	T_E	= 30.0°C
A	10^6 m	A	= 10^6 m ²
Time (Days)	Production Rate MMSCF/Year	Time (Days)	Production Rate MMSCF/Year
0.05	59,600	0.05	490,000
0.50	19,600	0.50	165,000
5.00	6,300	5.00	53,000
25.00	2,880	25.00	23,000
235.00	945	250.00	7,500
1365.00	397		

The conclusion to be drawn is that dissociation of gas hydrates is severely heat transfer limited after only the shortest periods of time. Even if the conductivities used in this example are not correct, it is clear that the presence of a medium between an injected hot fluid and the hydrate zone must be taken into account in calculating rates at which hydrates will dissociate.

7. Analysis of Reservoir Conditions where Hydrates are Likely to Form

Our computer program has been modified to generate hydrate stability data ^{some model!} in the earth. Below we present depth versus temperature charts for hydrate stability zones in the earth. The variables studied include

On land:

- Permafrost Thickness
- Geothermal Gradients
- Gas Composition
- Pressure Gradients

Beneath the Ocean:

- Ocean Depth
- Ocean Bottom Temperature"

oceanic as well?
is "ing" is:

These variables are cross-correlated so that any combination of permafrost thickness, gas composition and geothermal gradient can be included. Graphical correlations are presented below to show the effect that these variables have on hydrate zone thickness.

Results of the depth-temperature studies ^{all} is presented in several figures as outlined below. Table X shows the default values used for these calculations. They are considered to be representative values^{23,24} and where differences in values are likely, the effect^s of changes in these values have been given in Figures 29-39. Figure 29 shows the effect of a) permafrost thickness b) geothermal gradient below the hydrate zone and c) gas composition on the stability zone of hydrates in the earth. In these figures, the straight solid line extending downward from -10°C and zero depth gives the temperature depth profile in the earth for various permafrost thicknesses.

Figure 29: Temperature-Depth Profiles for Hydrate Stability Zones. I.

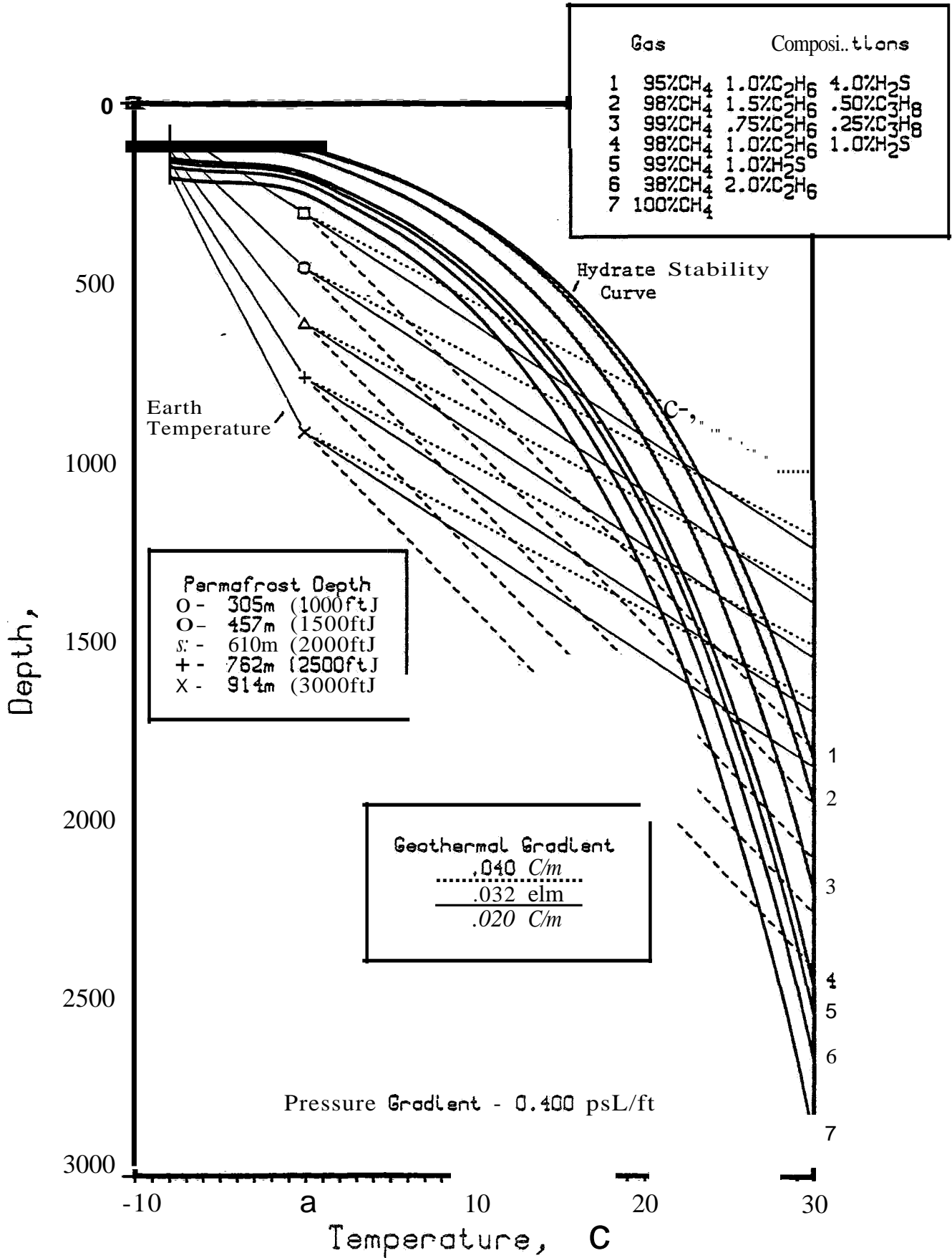


Figure 30: Temperature Depth Profiles for Hydrate Stability Zones, II.

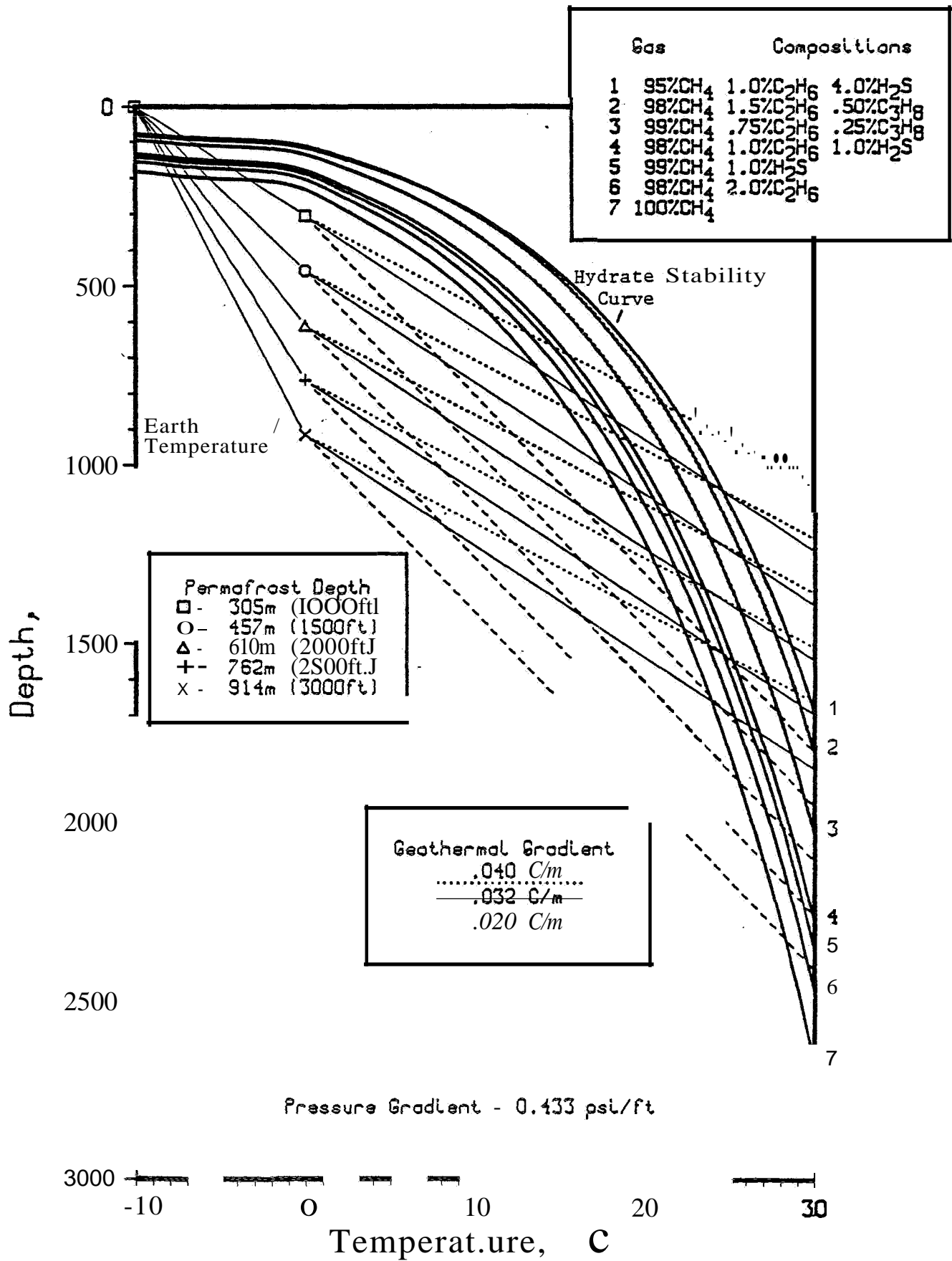


Figure 31: Temperature Depth Profiles for Hydrate Stability Zones, III.

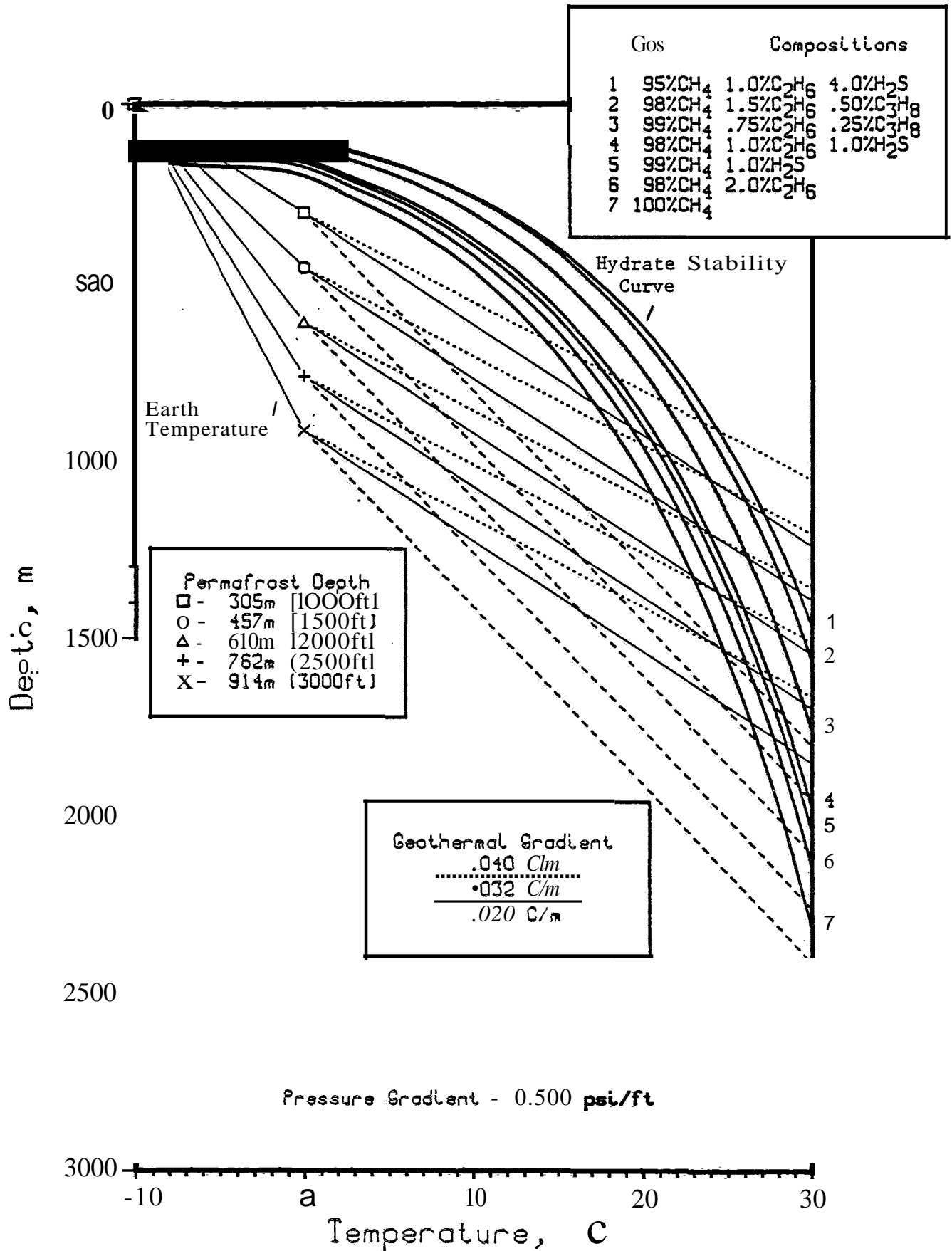


Figure 32: The Effect of the Geothermal Gradient Below the Permafrost on the Hydrate Stability Zone Beneath the Permafrost.

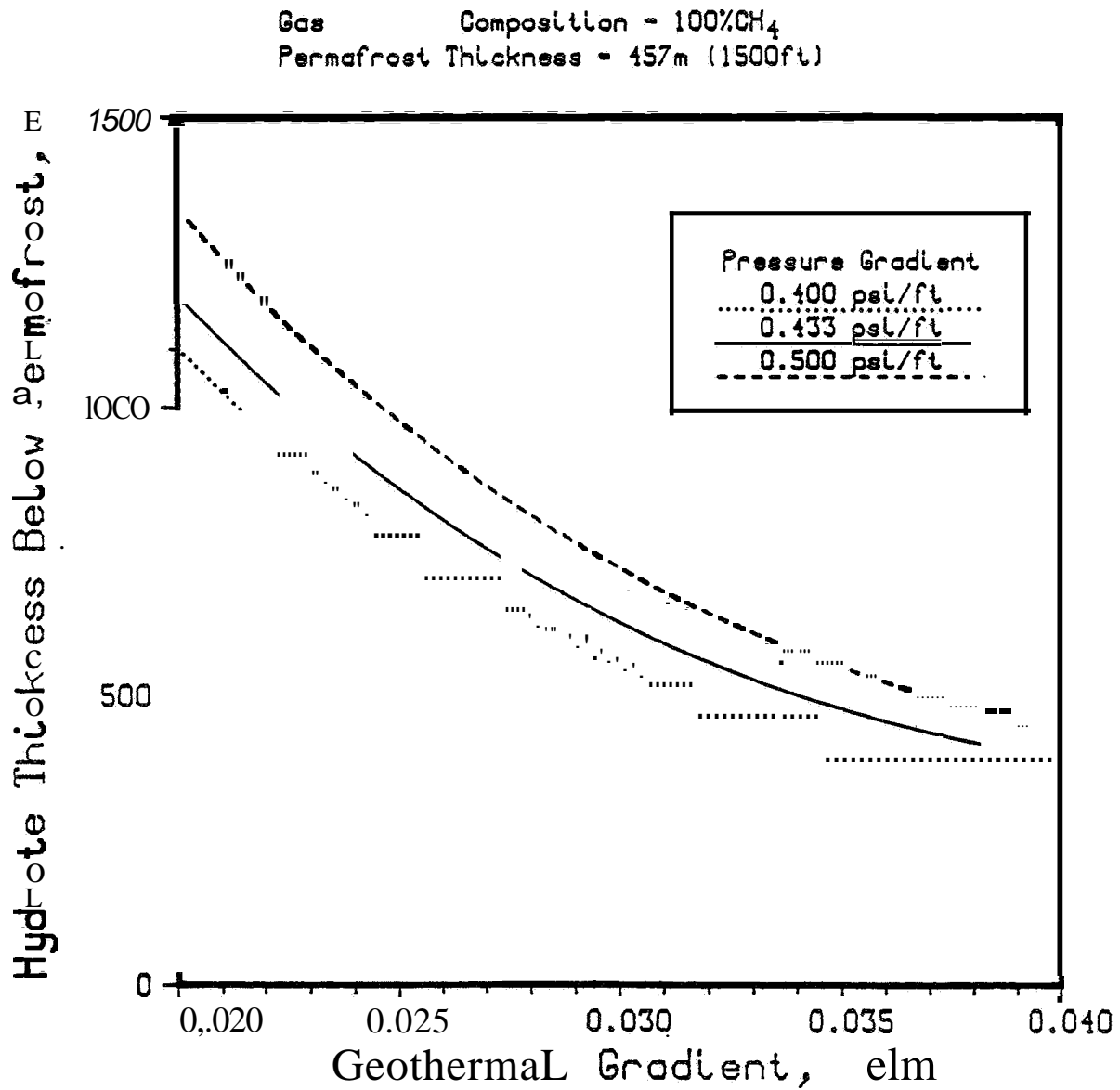


Figure 33: The Effect of Permafrost Thickness on the Hydrate Stability Zone Thickness in the Permafrost.

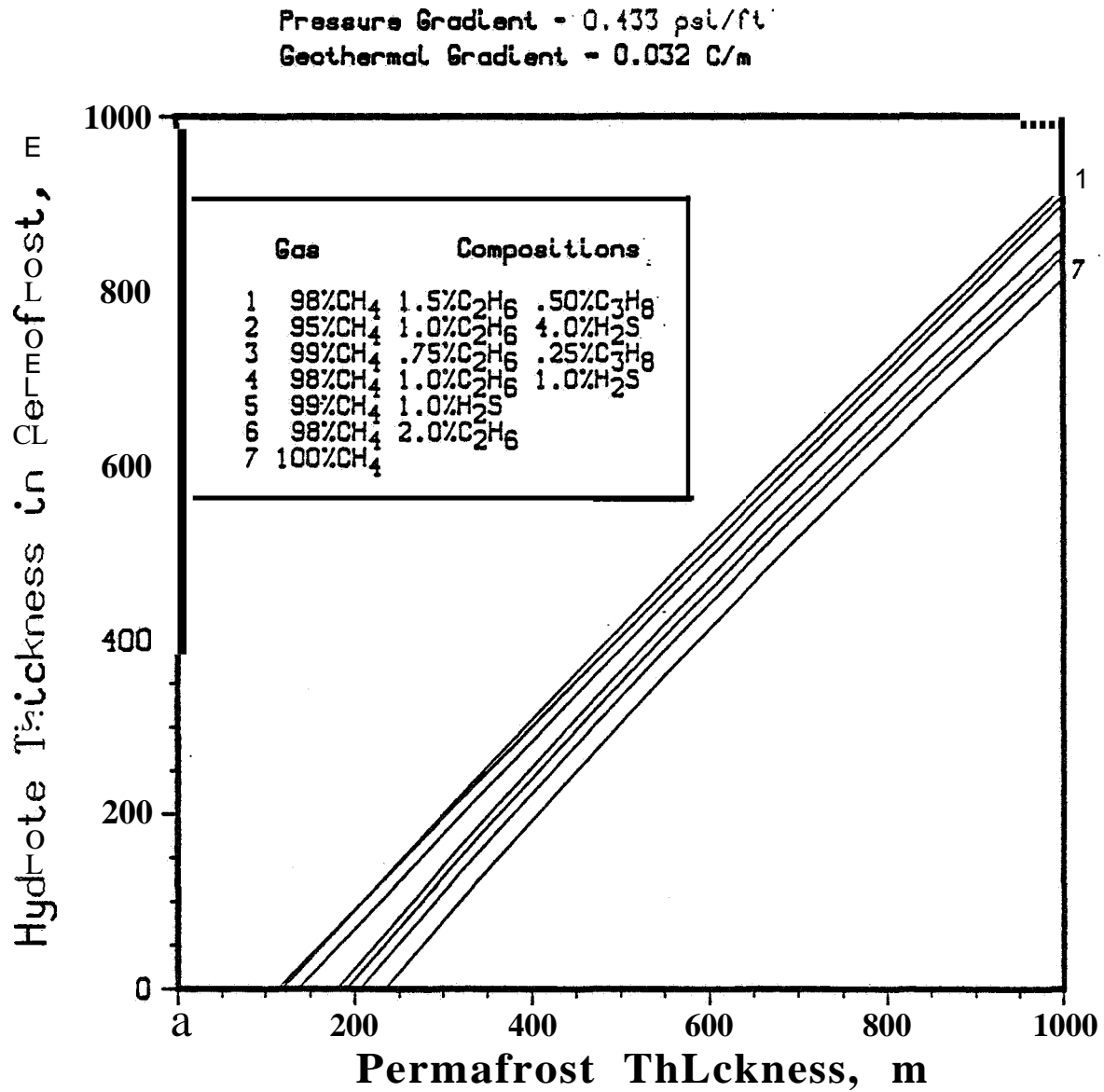


Figure 34: The Effect of Permafrost Thickness on the Thickness of the Hydrate Stability Zones for Seven Gas Compositions.

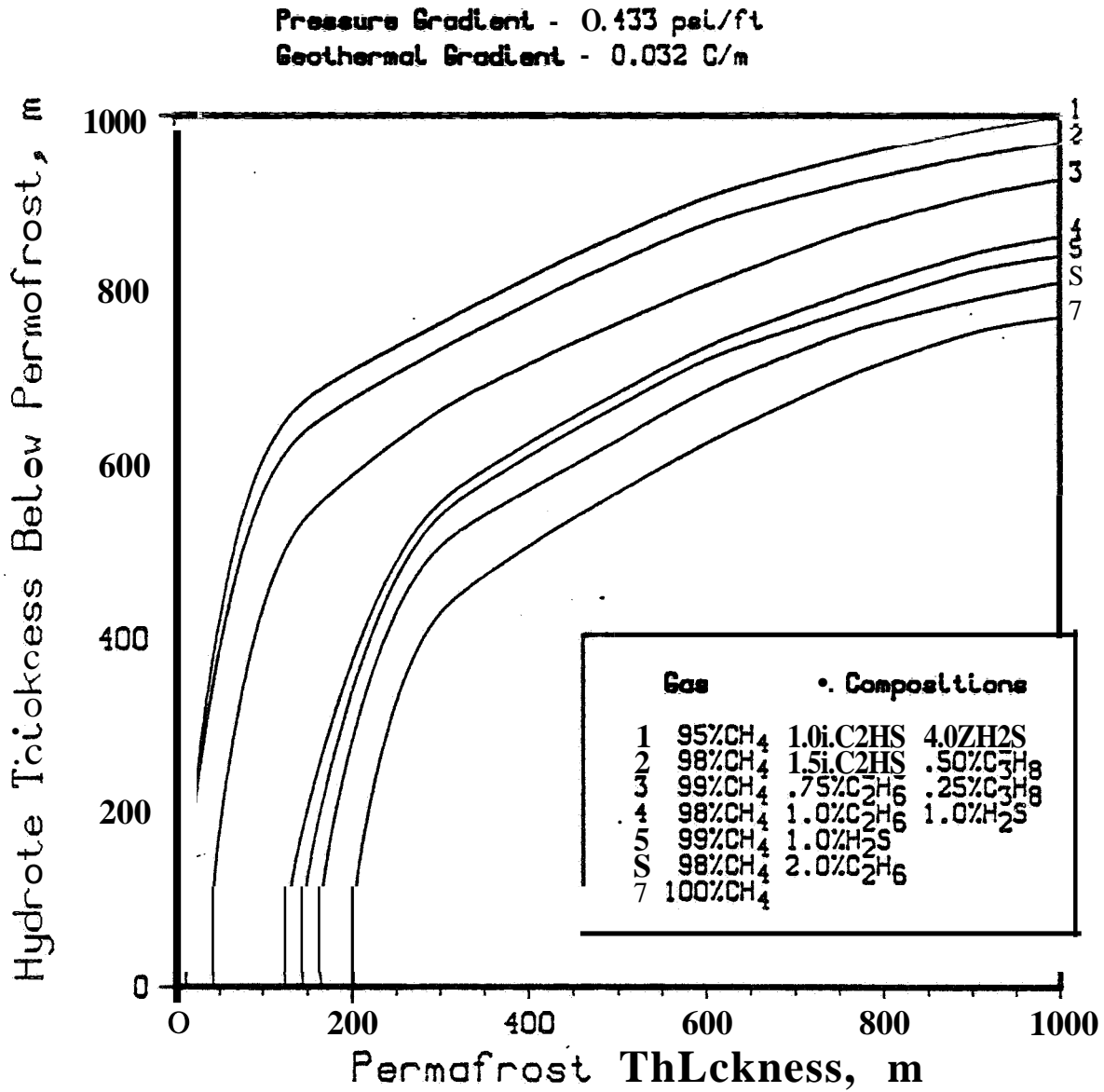


Figure 35: Depth-Temperature Profiles and Hydrate Stability Curves
Beneath the Ocean, I

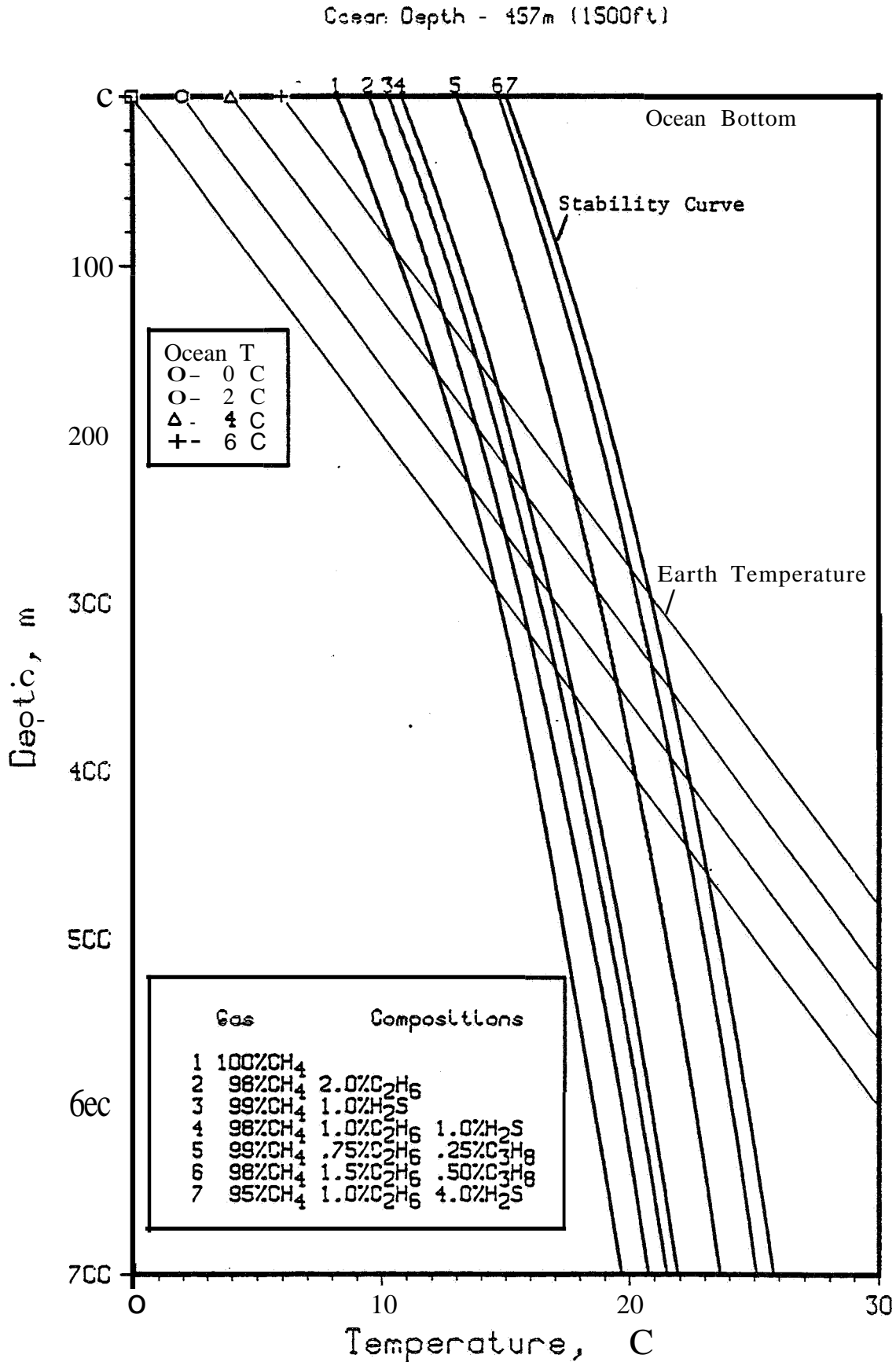


Figure 36: Depth-Temperature Profile and Hydrate Stability Curve, Beneath the Ocean, II.

Ocean Depth - 914m (3000ft)

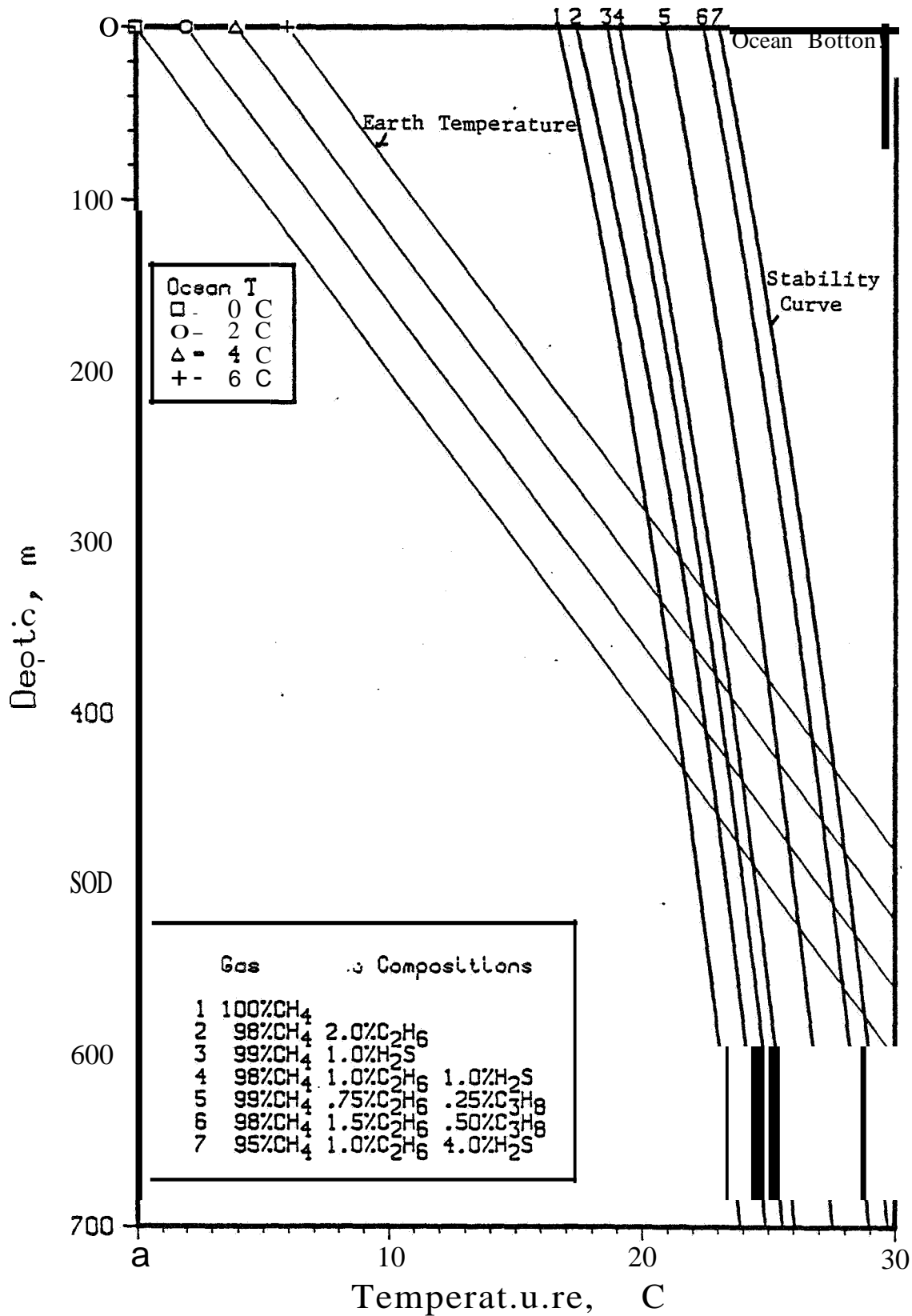


Figure 37: Depth-Temperature Profile and Hydrate" Stability Curves Beneath the Ocean, III.

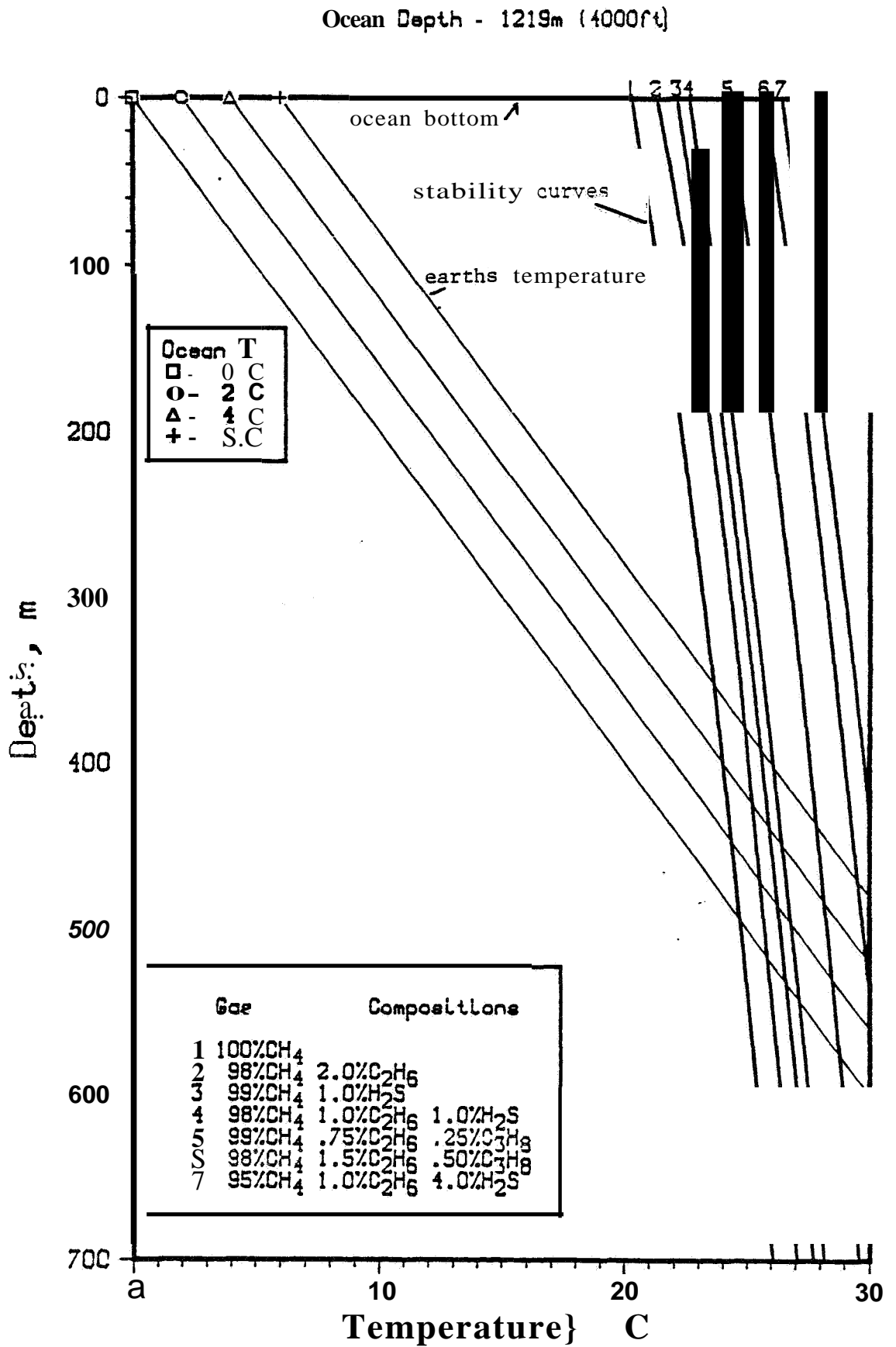


Figure 38: The Effect of the Ocean's Depth on the Hydrate Stability Zone Beneath the Ocean.

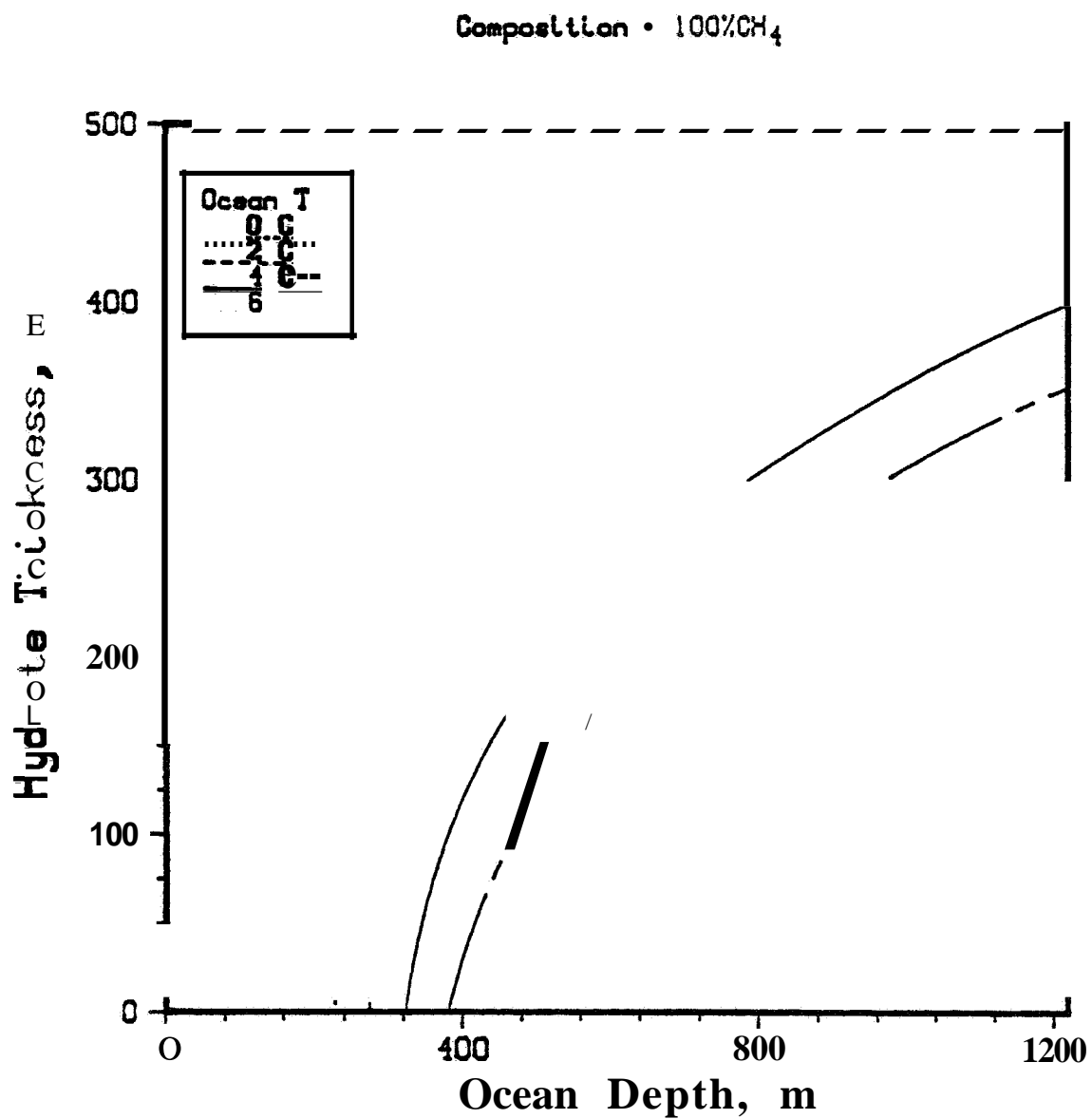


Figure 39: The Effect of Ocean Depth on the Thickness of the Zone of Hydrate Stability - Different Gas Compositions

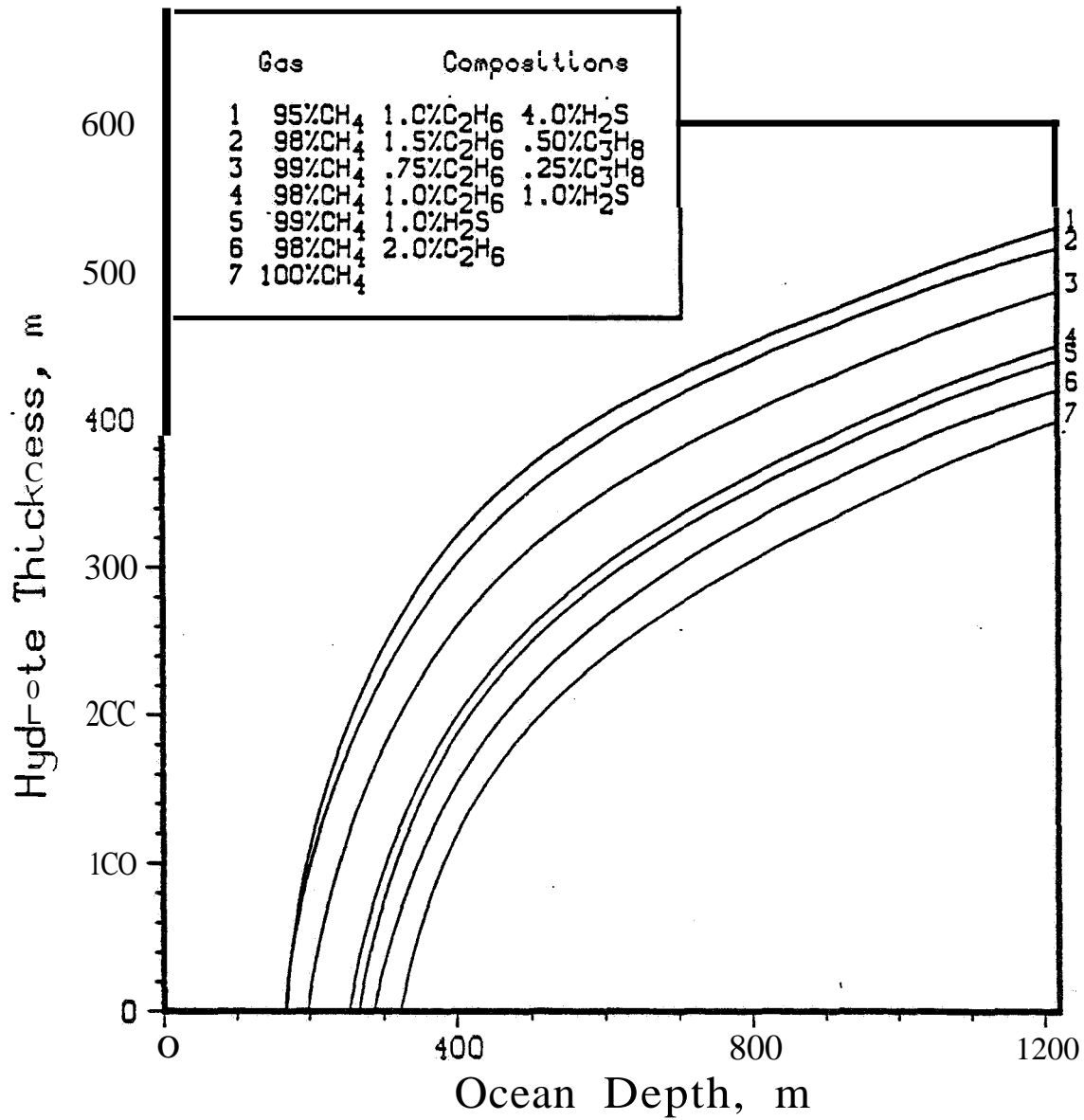


Table X: Default Values for Hydrate Stability Zone Calculations

Permafrost Thickness:	457 m (1500 ft)
Pressure Gradient:	0.433 psi/ft
Temperature Gradient:	0.032 °C/m
Surface Temperature:	-10°C
Gas Composition:	100% CH ₄
Permafrost Base Temperature:	00C
Ocean Bottom Temperature:	

The line ends at a symbol (□, ○, Δ, +, x) which indicates the base of the permafrost, each line representing a different permafrost thickness. From this base, three straight lines (dotted, solid and dashed) extend showing different possible depth-temperature profiles below the permafrost for geothermal gradients of .04, .032, and .020 °C/m respectively. Thus, this figure shows how temperature profiles in the earth might vary in regions of permafrost, and the lines show how the profiles depend on different permafrost thicknesses and geothermal gradients. Based upon the literature, we have assumed an effective average surface temperature of -10°C. This temperature and the depth of the permafrost base determine the geothermal gradient in the permafrost and thus this gradient is not an independent parameter.

The solid curved lines in this figure represent the hydrate stability temperature as a function of depth for different composition gases. If the earth's temperature is below this curve the hydrates are stable. For example, methane hydrates are stable between 200 meters and 2210 meters if the permafrost is 914 meters thick and the geothermal gradient is 0.020 °C/m. If, however, the permafrost is only 305 meters thick and the geothermal gradient

beneath the permafrost is $0.04\text{ }^{\circ}\text{C/m}$ then the zone of methane-hydrate stability is between 205 and 500 meters depth, about one sixth the size of the stability zone in the previous example.

Adding ethane (C_2H_6), hydrogen sulfide (H_2S) or propane (C_3H_8) increases the zone of stability dramatically. These gases and their compositions were chosen to cover the most likely range of gas compositions to be found in hydrate zones although others are certainly possible. Note that propane and H_2S have the greatest effect. Carbon dioxide would have an effect similar to that of ethane. Conditions do not vary linearly with pressure. Figure 30 is the same as Figure 29, but with a pressure gradient of 0.433 psi/ft . Note that the higher the pressure gradient, the greater the zone of stability. This gradient corresponds to a hydrostatic head and is the default value. Figure 31 is the same as Figure 29, but with a pressure gradient of 0.5 psi/ft which could occur if the pressure is not hydrostatically determined. Figures 29-30 can be used to determine the effect of the earth's pressure gradient.

Figure 32 shows the effect of geothermal gradient on the hydrate zone thickness below 457 meters of permafrost. It shows that the geothermal gradient is an extremely important variable in determining the zone of hydrate stability. The results are shown for the three different pressure gradients. Figure 33 shows how the hydrate thickness in the permafrost varies with permafrost thickness. There is essentially a linear relationship because most of the permafrost can form hydrates after about 200 meters of depth. Consequently, as the permafrost thickness increases so does the zone of stability in the permafrost. There is a compositional effect. Figure 34 shows how the depth of the permafrost affects the thickness of the hydrate stability zone beneath the permafrost. This relationship is highly non-linear and tends to level off as the permafrost thickness gets large.

Figure 35 shows the Depth-Temperature Profile in the earth--for different ocean bottom temperatures (0, 2, 4, 6 °C). Overlain are the temperature-depth stability profiles for gases of several different compositions. For any given pair of earth-temperature and stability curves, hydrates are stable from the ocean bottom to the depth at which the two curves intersect. For example, a gas containing 2% ethane and 98% methane will form hydrates to 110 meters depth if the ocean bottom temperature is 6 °C and to 305 meters depth if the ocean bottom temperature is 0°C. Even though the F-T conditions are appropriate, it is very unlikely that hydrates would be present; right at the ocean bottom since the ocean would wash them away. Figure 36 is the same as Figure 35 except the ocean depth is 914 meters. Figure 37 is the same as Figure 35 except the ocean depth is 1219 meters. Note that the zone of stability increases as ocean depth increases. This is because the increased pressure increases the temperature required to melt the hydrates. In all calculations the pressure gradients used are 0.433 psi/ft. The depth of the ocean must be added to the depth beneath the ocean bottom to calculate the insitu pressure.

Figure 38 shows the effect of ocean depth on the thickness of the hydrate stability zone under the ocean bottom. It depends upon the temperature at the bottom of the ocean (0, 2, 4, or 6 °C were used). The deeper the ocean and the colder the ocean bottom, the greater is the zone of hydrate stability. Figure 39 is similar. It shows how gas composition affects the thickness of the hydrate stability zone.

This part of the report has covered the effect of gas composition, geothermal gradient, permafrost thickness and pressure gradient on the thickness of a hydrate stability zone in permafrost regions. It also shows the effect of ocean bottom temperature, gas composition and ocean depth on a

hydrate stability zone beneath the ocean. These variables are considered to be ~~among the more important~~ in determining the potential that a particular region has for containing hydrates, and they need to be measured in any geological investigation of a region.

8. Advice and Consultation

During the months of September and October, efforts were spent on Item 8 (advice and consultation) with regard to experiments on the methane-hydrate core sample that was obtained from Denny Sloan at the Colorado School of Mines. It was noted that this core appeared to be much more stable (stability means that the hydrates do not decompose rapidly when exposed to an ambient environment) than the synthetic cores produced in my LaboratorLas at the University of Pittsburgh. One reason for this greater stability is the greater compression that these cores have undergone. The synthetic laboratory cores are formed at pressures near 1000 psia while the natural cores were formed at pressures near 3200 psia. Similarly, the porosity of the synthetic cores is about 40-50%, while the porosity of the natural core is probably less (about 10-30%. I would guess).

A second and probably more significant difference is the ¹⁰⁵ pUritf of the ^{gases in} ~~natural~~ ^{synthetic} and natural cores ^{aa.} ~~is~~ probably considerably different. In the natural cores, nearly 100% ^{← how do you know this?} of the water is converted to hydrate. For the core at METC, the amount of water converted to hydrate is not known and it is my recommendation that it be measured. The measurement should determine the mass of water (M_{H_2O}), the volume of gas at standard conditions (V), the mass of sediment (M_s). The mass of water in the hydrate phase (M_H) will then be:

$$\frac{(6.1S)(18)V}{22.400} \quad V = \text{cc of gas} \quad (8-1)$$

The percentage of water in the hydrate phase will be:

$$\% \text{ Hydrate} = \frac{M_H}{M_{H_2O}} (100) \quad (8-2)$$

Additional advtce has been provided orally during visits to Morgantown over the past year.

References

1. Makogen, Y.F., Gazovaya Promyshlennost 5 1965.
2. Meyer, R.F., IIASA Conference on Conventional and Unconventional World Natural Gas Resources, Fourth Conference, Montreal, Canada 1979.
3. Dobrynin, V.M., KorotaJer, Y.P. and Plyushev, D.V., IIASA Conference on Conventional and Unconventional World Natural Gas Resources, Fourth Conference, Montreal, Canada, °1979.
4. McIver, R.D., Proceedings from the UNITAR Conference on Long-Term Energy Resources, Montreal, Canada 2 (3): 13 1979.
5. Claussen, W.F., J. of Chem. Phys., 1951 19 1979.
6. Pauling, L. and March, R.E., National Academy of Science Proceedings, 1952 28, 112.
7. Stac:kelberg, Von M. and Muller, H.R., Zeit Electrochemistry, 1954 58, 25.
8. Byk, S. She and Fomina, V.I., Russian Chemical Reviews, 1968 37 (6) 469.
9. Holder, G.D. and Hand, J.R., ArChE J., 1982 28 (3) 440.
10. Wu, B.J., Robinson, D.B. and Ng, R.J., J. Chem. Thermodynamics, 1976 8, 461.
11. Barrer, R.M. and Ruzicka, D.J., Trans. Soc. 1962 58, 2239.
12. Holder, G.D., Corbin, D. and Papdopoulos, K.D., I. and E.C. Fundamentals, 1980 19, 2828.
13. Makogen, Y.F., "Hudrates of Natural Gas," (1974), Translated by Cieslewicz, W.J., Geexplorer Association Inc., Denver, Colorado 1978.
14. Bily, C. and Dick, J.W.L., Bull. Can. Pet. Geo., 1974 22, 340.
15. Makogen, Y.F., Tsarev, V.P. and Chersky, N.V., Dokladr-Earth Sci. Sec. 1972 205, 215.
16. Rolder, G.D., Angert, P.F. and Godbole, S.P. "Simulation of Gas Production From A Reservoir Containing Both Gas and Free Natural Gas," Proc. Soc. Pet. Engr.Meeting, New Orleans, LA. SPE 11105, Nov. 1982.
17. McGuire, R.L., Los Alamos National Laboratory, LA-9162-M.S., Nov. 1981.
18. Knox, W.G., Hess, M., Jones, G.E., Smith, R.B., "The Rydrate Process," Chem. Eng. Prog., 57 (2): 66 1961.
19. Barrer, R.M. and RUZicka, D.J., "Non-Stoichiometric Clathrate Compounds of Water," Trans. Faraday Soc. 58 (4): 2262 1962.

20. Barrer, R.M. and Stuart, W.I., "Gas Hydrates Containing Argon, Krypton and Xenon: Kinetics and Energetics of Formation and Equilibria," Proc. Roy. Soc. (London), A2453: 172 1958.
21. Vysniauskas, A. and Bishnoi, P.R., "A Kinetic Study of Methane Hydrate Formation," Chem. Eng. Sci., 38 (7): 1061 1983.
22. Chiew, Y.C. and Glandt, E.D., "The Effect of Structure on the Conductivity of a Dispersion," J. Colloid and Interface Science, 94 (1): 90 1983.
23. Holder, G.D., Katz, D.L., Hand, J.H., "Am. Assoc. of Pet. Geo. Bull. 60 (6), 981(1976).
24. Collet, T.S., "Detection and Evaluation of Natural Gas Hydrates from Well Logs," Prudhoe Bay, Alaska, M.S. Thesis, University of Alaska, Fairbanks, 1983.